

Development of the SSiB5/TRIFFID/DayCent-SOM Model and study of the impacts of nitrogen dynamics on terrestrial carbon cycle

zheng xiang^{1,1}, Yongkang Xue^{2,2}, Weidong Guo^{3,3}, Melannie Hartman^{4,4}, Ye Liu^{5,5}, and Bill Julian Parton^{6,6}

¹Nanjing University

²University of California Los Angeles

³Institute for Climate and Global Change Research, School of Atmospheric Sciences, Nanjing University

⁴Natural Resource Ecology Laboratory

⁵Pacific Northwest National Laboratory (DOE)

⁶CSU

January 20, 2023

Abstract

Plant and microbial nitrogen (N) dynamics and nitrogen availability regulate the photosynthetic capacity and capture, allocation, turnover of carbon (C) in terrestrial ecosystem. It is important to adequately represent plant N processes in land surface models. In this study, a plant C-N framework was developed by coupling a biophysical and dynamic land surface processes model, SSiB4/TRIFFID, with a soil organic matter cycling model, DayCent-SOM, to fully incorporate N regulations to investigate the impact of N on plant growth and C cycling. To incorporate the N limitation in the coupled system, the parameterization for dynamic C/N ratios for each plant functional type (PFT) was developed first. Then, after accounting for plant/soil N-cycling, when available N is less than demand, N would restrict the plant growth, reducing the net primary productivity (NPP), but also impact plant respiration rates and phenology. The improvements of the newly-developed model, the SSiB5/TRIFFID/DayCent-SOM, was preliminary verified at three flux tower sites with different PFTs. Furthermore, several offline global simulations were conducted from 1948 to 2007 to predict the long-term mean vegetation distribution and terrestrial C cycling, and the results are evaluated with satellite-derived observational data. The sensitivity of the terrestrial C cycle to N processes is also assessed. In general, new model can better reproduce observed emergent properties, including gross primary productivity (GPP), leaf area index (LAI), and respiration. The main improvements occur in tropical Africa and boreal regions, accompanied by a decrease of the bias in global GPP and LAI by 16.3% and 27.1%, respectively.

Zheng Xiang^{1,2}, Yongkang Xue^{2*}, Weidong Guo^{1,4*}, Melannie D. Hartman³, Ye Liu², William J. Parton³

¹School of Atmospheric Sciences, Nanjing University, Nanjing, China

²Department of Geography, University of California, Los Angeles, CA 90095, USA

³Natural Resource Ecology Laboratory, Colorado State University, CO 80523, USA

⁴Joint International Research Laboratory of Atmospheric and Earth System Sciences, Nanjing, China

Correspondence to: Yongkang Xue (yxue@geog.ucla.edu), Weidong Guo (guowd@nju.edu.cn)

Key Points:

- Developed a process-based C-N coupling approach by incorporating plant C-N framework for modeling territorial biogeochemical cycles
- Compared to observations, newly developed SSiB5/TRIFFID/DayCent-SOM model produces better GPP and LAI than the model without N process

Abstract

Plant and microbial nitrogen (N) dynamics and nitrogen availability regulate the photosynthetic capacity and capture, allocation, turnover of carbon (C) in terrestrial ecosystem. It is important to adequately represent plant N processes in land surface models. In this study, a plant C-N framework was developed by coupling a biophysical and dynamic land surface processes model, SSiB4/TRIFFID, with a soil organic matter cycling model, DayCent-SOM, to fully incorporate N regulations to investigate the impact of N on plant growth and C cycling. To incorporate the N limitation in the coupled system, the parameterization for dynamic C/N ratios for each plant functional type (PFT) was developed first. Then, after accounting for plant/soil N-cycling, when available N is less than demand, N would restrict the plant growth, reducing the net primary productivity (NPP), but also impact plant respiration rates and phenology. The improvements of the newly-developed model, the SSiB5/TRIFFID/DayCent-SOM, was preliminary verified at three flux tower sites with different PFTs. Furthermore, several offline global simulations were conducted from 1948 to 2007 to predict the long-term mean vegetation distribution and terrestrial C cycling, and the results are evaluated with satellite-derived observational data. The sensitivity of the terrestrial C cycle to N processes is also assessed. In general, new model can better reproduce observed emergent properties, including gross primary productivity (GPP), leaf area index (LAI), and respiration. The main improvements occur in tropical Africa and boreal regions, accompanied by a decrease of the bias in global GPP and LAI by 16.3% and 27.1%, respectively.

Plain Language Summary

Adequate representation of nitrogen cycle is crucial for climate models to produce proper responses of terrestrial ecosystem to higher atmospheric CO₂ and global warming. In this study, a biogeochemical module was introduced to represent soil organic matter cycling and the availability of plant nitrogen uptake from soil. A plant carbon-nitrogen framework was developed for modeling interactions between carbon and nitrogen processes, and regulates photosynthesis, respiration, and plant phenology. Moreover, instead of fixed carbon/nitrogen ratio as done by many other studies, a dynamic carbon/nitrogen ratio is introduced based on nitrogen availability. A series of numerical experiments are carried out, and the results show that the model with nitrogen process can better produce monthly mean gross primary productivity, leaf area index, and global nitrogen-limitation patterns.

1 Introduction

Land surface processes substantially affect climate (Foley et al., 1998; Ma et al., 2013; Sellers et al., 1986; Xue et al., 2004, 2010) and are influenced by climate in turn (Bonan, 2008; Liu et al., 2019a; Zhang et al., 2015), forming complex feedback loops to climate change (Friedlingstein et al., 2006; Gregory et al., 2009). To study these processes, the land surface components of Earth System Models (ESMs) have evolved from one that only represents biophysical processes (i.e., hydrology and energy cycle) to include terrestrial carbon (C) cycle, vegetation dynamics, and nutrient processes (Cox et al., 2001; Dan et al., 2020; Foley et al., 1998; Jiang et al., 2014; Lu et al., 2001; Niu et al., 2020; Oleson et al., 2013; Pan et al., 2017; Sellers et al., 1986; Sitch et al., 2003; Wang et al., 2010a; Yang et al., 2019). Current land surface models have large uncertainties in predicting historical and nowadays C exchanges (Beer et al., 2010; Richardson et al., 2012; Zaehle et al., 2015), which has been criticized for being unjustified from an ecological point of view (Reich et al., 2006) and for overestimating terrestrial C sequestration in the future (Hungate et al., 2003; Thornton et al., 2007). The differences in predictions using land models have been attributed to many factors. The inclusion or exclusion of nutrient limitations on productivity is one of the critical factors. Those C-only models ignore significant nitrogen (N) limitation and therefore overestimate carbon sequestration by terrestrial ecosystems under climate change (Peñuelas et al., 2013; Zaehle et al., 2015).

Ecosystem N cycling processes are among dominant drivers of terrestrial C-climate interactions through their impacts, mainly N-limitation, on vegetation growth and productivity (Reich et al., 2006), especially in nitrogen-poor younger soils in high latitudes (LeBauer & Treseder, 2008; Vitousek & Howarth, 1991), and on microbial decomposition of organic matter (Hu et al., 2001). The need to represent soil organic matter (SOM) cycling and N-limitation to plant and microbial processes led to the development of CENTURY (Parton et al., 1988) and DayCent model (Parton et al., 1998; 2010) that operates at a daily time step instead of the original monthly time step, and includes soil nitrification/denitrification processes. Another biogeochemical model, the Fixation and

Uptake of Nitrogen (FUN) model (Fisher et al., 2010), expands plant N acquisition to include passive uptake, active uptake, re-translocation, and symbiotic N-fixation through a carbon cost.

The N cycle and its effect on C uptake in the terrestrial biosphere in land surface models (LSMs) is a recent progress of ESMs (Davies-Barnard et al., 2020), and various representations of N processes have been included in ESMs (Ali et al., 2015; Best et al., 2011; Clark et al., 2011; Ghimire et al., 2016; Goll et al., 2017; Krinner et al., 2005; Matson et al., 2002; Oleson et al., 2013; Thum et al., 2019; Wang et al., 2010; Yu et al., 2020; Zhu et al., 2019). The latest Coupled Model Intercomparison Project Phase 6 (CMIP6, Eyring et al., 2016) has about 10 models that incorporate the N cycle (Arora et al., 2020). Among these models, by coupling a terrestrial biogeochemistry model, Biome-BGC (Thornton et al., 2007, 2009), the Community Land Model version 4 (CLM4; Oleson et al., 2010) was the first N model in a ESM used in the CMIP6. In the CMIP6, the CLM5 (Lawrence et al., 2019) implements a C cost basis for acquiring N, derived from the FUN approach (Fisher et al., 2010). The Lund-Potsdam-Jena General Ecosystem Simulator version 4.0 (LPJ-GUESS; Smith et al., 2014) incorporates a SOM cycling scheme adopted from the CENTURY model (Parton et al., 1993) to simulate C and N dynamics and produce N-limitation map. The SURFEX (Surface Externalisée, Le Moigne, 2018) also employs CENTURY to simulate soil C and N dynamics. Some other modelling studies have also reported improvements in simulated C stocks and fluxes by introducing N processes. For instance, by considering the N cycle, the Joint UK Land Environment Simulator version 5.1 (JULES-CN, Wiltshire et al., 2020) found nutrient limitation reduces carbon-use efficiency. After introducing N cycling, the SURFEX represented the terrestrial carbon cycle in a more realistic way (Le Moigne, 2018). Moreover, the implementation of CO₂-induced nutrient limitation (CNL, Goll et al., 2012) and a decomposition model (YASSO) help the JSBACH model (Goll et al., 2017) reduce accumulated land carbon uptake.

Despite the recent progress, coupling of N process is still in the early developing stage as can be seen from above brief review. In the latest CMIP6 (Eyring et al., 2016), although there were 112 different versions of coupled models with various land surface models from 33 research teams, only about 10 models incorporated the N cycle module (Arora et al., 2020) with various deficiency, which indicates an imperative need for substantially more research on this subject. A few key N processes, such as N limitation on GPP, the effect of biomass N content on autotrophic respiration, plant N uptake, ecosystem N loss and biological N fixation, have been introduced into LSMs with various complexity and selected components. This paper mainly focuses on the N limitation effect, which has been presented in current land models with different approaches, including using N to scale down photosynthesis parameter $V_{c,max}$ (Ghimire et al., 2016; Zaehle et al., 2015) or potential GPP to reflect N availability (Gerber et al., 2010; Oleson et al., 2013; Wang et al., 2010a); defining a C cost of N uptake (Fisher et al., 2010); optimizing N allocation for leaf processes (Ali et al., 2015); and adapting a flexible C/N ratio for N allocation (Ghimire et al.,

2016). In many of these approaches, N limitation is represented as instantaneous down-regulation of potential photosynthesis rates based on soil mineral N availability. Moreover, the plant C/N ratio is a key concept in presenting the C/N interactions. However, many land models specify fixed plant C/N ratios for each plant functional type (PFT) (e.g., Best et al., 2011; Clark et al., 2011; Krinner et al., 2005; Oleson et al., 2013; Wang et al., 2010b). As a matter of fact, plant C/N ratios change over the plant’s lifecycle as well as with nutrient availability, and flexible plant C/N ratios are not represented in many models.

In this paper, we present a newly developed LSM, in which the potential N uptake depends on plant demand from a biophysical and dynamic vegetation model, SSiB5/TRIFFID (The Simplified Simple Biosphere Model version 5/ the Top-down Representation of Interactive Foliage and Flora Including Dynamics Model, Cox, 2001; Harper et al., 2016; Liu et al., 2019; Xue et al., 1991; Zhan et al., 2003; Zhang et al., 2015). And the actual N uptake is limited based on C:N stoichiometry in the plant and N availability in the soil output from the SOM cycling portion of the DayCent model, DayCent-SOM (Del Grosso et al., 2000; Parton et al., 1998; 2010). A plant C-N framework, which regulates photosynthesis, respiration, and plant phenology, as well as makes a consistent biophysical process and biogeochemical process coupling, is introduced to couple DayCent-SOM into SSiB5/TRIFFID. This plant C-N framework is central to the newly coupled model, SSiB5/TRIFFID/DayCent-SOM, and includes flexible C/N ratios depending on whether the N demands of different plant organs (e.g., leaf, root, and wood) are satisfied. Using this dynamic C/N ratio, SSiB5/TRIFFID/DayCent-SOM can simulate the plant resistance and prevent unrealistic instantaneous down-regulation of potential photosynthesis rates. This new strategy presents the limitation of N on plant-N-related respiration rates and phenology changes. This model development incorporates DayCent’s strength in parameterizations of symbiotic biological N fixation, N mineralization/immobilization, nitrification/denitrification, N-gas emissions, atmospheric N deposition, and nitrate leaching. The coupled model was verified at three flux tower sites with different PFTs and was used to conduct several sets of global offline simulations from 1948 to 2007. The model predictions of GPP and LAI are evaluated against satellite-derived observational data. The results demonstrate the relative importance of different N processes in the plant C-N framework. The model and coupling are presented in section 2. In section 3, The development of SSiB5/TRIFFID/DayCent-SOM model is presented. A preliminary test with three site measurements is presented in section 4. Data and experimental design are reported in section 5. In section 6, the model performance in predicting the global vegetation distribution and terrestrial C cycling based on long term simulation are evaluated using satellite products. Some issues and conclusion are presented in section 7.

2 Models and Coupling Strategy

2.1 SSiB4/TRIFFID model

The Simplified Simple Biosphere Model (SSiB, Xue et al., 1991; Sun and Xue,

2001; Zhan et al., 2003) is a biophysical model that simulates fluxes of surface radiation, momentum, and sensible/latent heat, runoff, soil moisture and temperature, and vegetation GPP based on energy and water balance and photosynthesis processes. The SSiB was coupled with a dynamic vegetation model, the Top-down Representation of Interactive Foliage and Flora Including Dynamics Model (TRIFFID), to calculate NPP, LAI, canopy height, and PFT fractional coverage according to the C balance (Cox, 2001; Harper et al., 2016; Liu et al., 2019; Zhang et al., 2015). Moreover, the surface albedo and aerodynamics resistances are also updated based on the vegetation conditions. The previous work has improved the PFT competition strategy and plant physiology processes to make the SSiB4/TRIFFID suitable for seasonal, interannual, and decadal studies (Zhang et al., 2015). SSiB4/TRIFFID includes seven PFTs: (1) broadleaf evergreen trees (BET), (2) needleleaf evergreen trees (NET), (3) broadleaf deciduous trees (BDT), (4) C3 grasses, (5) C4 plants, (6) shrubs, and (7) tundra. A PFT coverage is determined by net C availability, competition between species, and disturbance, which includes mortality due to fires, pests, and windthrow. A detailed description and validation of SSiB4/TRIFFID can be found in Zhang et al., (2015); Liu et al., (2019) and Huang et al., (2020).

2.2 DayCent model

DayCent is a daily version of the CENTURY ecosystem model (Parton et al., 1998; Del Grosso et al., 2000). The model simulates major processes associated with C, N, phosphorus (P), and sulfur (S) cycling in a plant-soil system. The model also simulates agriculture land management practices, such as grazing, irrigation, cultivation, residue removal during harvest, organic matter and chemical fertilizer additions, and flooding and drainage. Key processes include decomposition of litter and SOM; mineralization/immobilization and plant uptake of nutrients; N-gas emissions from nitrification and denitrification; and CH_4 oxidation in non-saturated soils (i.e., methanotrophy). Litter and SOM decomposition is controlled by soil moisture, temperature, pH, and tillage intensity. Model inputs are daily weather data (e.g., maximum and minimum air temperature, precipitation, solar radiation, wind speed, and relative humidity), soil properties, and land management and disturbance data (e.g. fire, biomass harvest, flooding, and storm damage). The DayCent model has been used to simulate NPP, soil organic C, N_2O emissions, nitrate leaching, and CH_4 oxidation in various native and managed systems with extensive validations (Del Grosso et al., 2000, 2005; Parton et al., 2010).

Only DayCent’s SOM cycling functions (DayCent-SOM) are coupled with the SSiB5/TRIFFID. DayCent-SOM includes five types of organic C and N pools consisting of two plant litter pools (metabolic and structural) and three kinetically defined organic matter pools, (active, slow, and passive); all organic pools except the passive pool have both above-ground and below-ground counterparts. DayCent-SOM is forced with soil temperature and soil moisture, and plant C and N litter inputs from SSiB4/TRIFFID, computes daily changes to all organic matter and mineral soil pools, estimates losses of N from nitrate leaching and

N_2O , NO_x , and N_2 emissions, estimates the amount of inorganic N available to plants (N_{avail}), and updates inorganic N pools based on plant N-uptake. The full description for plant N uptake and soil N dynamics is available in Parton et al. (1994, 1998) and Del Grosso et al. (2000).

2.3 Coupling strategy – a plant Carbon-Nitrogen (C-N) Interface framework

To represent C/N interactions in SSiB5/TRIFFID/DayCent-SOM, we have developed a plant C-N interface framework to take into account both biophysical and biochemical C/N processes in plant life activities. The conceptual considerations in developing this framework are presented in this section. As a process-based model, we have to introduce a consistent coupling philosophy between biophysical and biogeochemical processes. The DayCent-SOM is directly driven by soil temperature/moisture as well as plant C/N litter into soil. Because the surface water, radiation, and carbon fluxes and plant litter are calculated by SSiB5, we turn off the soil temperature and soil moisture module in the DayCent-SOM, and use SSiB5-produced soil temperature and soil moisture, and plant litter to drive the DayCent-SOM. The DayCent-SOM then computes daily changes of all organic matter and mineral soil pools, estimates losses of N from nitrate leaching and N_2O , NO_x , and N_2 emissions, predicts the amount of inorganic N available to plants, and eventually updates inorganic N pools for SSiB. On the basis of plant N-uptake from DayCent-SOM, our plant C-N interface framework describes N effects on plant physiology from the following aspects: photosynthesis, plant autotrophic respiration, and plant phenology plus a dynamical C/N ratio (Fig. 1). Following such model development philosophy, we try to more realistically represent the physiological processes of N cycling. This approach takes into account both biophysical and biochemical N processes in plant life activities with unique features among current LSMs in C-N coupling.

A commonly used parameterization of photosynthetic C assimilation by the terrestrial biosphere in ESMs is represented by the Farquhar, von Caemmerer, and Berry (FvCB) model of photosynthesis (Collatz et al., 1991; Farquhar et al., 1980). Plants require N as essential components of photosynthetic proteins involved in light capture, electron transport, and carboxylation (Evans, 1989). Nitrogen is an important constituent of Rubisco enzyme and mitochondrial enzymes that regulate respiration and adenosine triphosphate (ATP) generation (Makino & Osmond, 1991). One of the most important photosynthetic model parameters, the maximum carboxylation rate by the Rubisco enzyme ($V_{c,\text{max}}$) is a key parameter in the FvCB model (Farquhar et al., 1980), and has an extensive range across the models depending on the plant N content (Rogers, 2014). Since N is an important component of Rubisco enzyme, leaf N content will affect $V_{c,\text{max}}$ thus GPP. The original FvCB model has not explicitly considered the N effect on the plant C; while in a number of LSMs an empirical relationship is applied to relate $V_{c,\text{max}}$ to leaf N content N_{leaf} to generate the effect of N on photosynthesis, e.g., $V_{c,\text{max}} = i_v + s_v \times N_{\text{leaf}}$, where the intercept (i_v) and

slope (s_v) are derived for each PFT based on observations (Kattge et al., 2009; Raddatz et al., 2007). Moreover, for plant N processes, normally, only the relationship between the root N uptake and GPP/NPP is considered to represent the N-limitation on C cycles (Ali et al., 2015; Fisher et al., 2010; Ghimire et al., 2016). However, because NPP is the difference between GPP and autotrophic respiration, adjusting NPP or GPP only may cause the ratio between NPP and respiration to deviate from reality. Using process-based N-limitation factor produced from DayCent-SOM to modify $V_{c,max}$ (See section 3.3) is an approach in our C-N interface framework and should be a more realistic way to produce the N effect on photosynthesis process.

In the SSiB4/TRIFFID, with the assumed unlimited N availability, fixed C/N ratios and assimilated C determine nitrogen contents of leaf, stem, and root, then respiration, which influences GPP, LAI, and NPP. The C/N ratio is specified based on PFTs. However, there is evidence that plants can adjust their resources and stoichiometric requirements. Changes in N resource availability will result in changes to plant C allocation and partitioning. Studies show plants resorb only about 50% of leaf N on average (Aerts, 1996) to conserve nutrients (Clarkson & Hanson, 1980), and to increase nutrient use efficiency (Herbert & Fownes, 1999; Vitousek, 1982). These processes cause a major internal nutrient flux and changes of C/N ratios to reduce the impact of nitrogen limitation (Talhelm et al., 2011; Vicca et al., 2012). In addition, plant responses, such as plant resistance and self-adjustment, will be limited under fixed C/N ratios, which affect plant productivity and change litter N content, thus drive changes in the underground biogeochemistry and ultimately C and N uptake and storage (Drewniak & Gonzalez-Meler, 2017). A study on the N deposition effect shows that the increase in foliar N under increased N, would improve model responses because it allows adaptations in the stoichiometry of C and N (Medlyn et al., 2015). The main impact of this will be to decrease C/N ratio in leaves, driving increases in productivity and changes soil and litter N content. A dynamic C/N ratio is employed in our framework to more realistically obtain N states and properly represent the effect of N processes (See section 3.2 for more details).

Nitrogen is not only a dominant regulator of vegetation dynamics, GPP/NPP, and terrestrial C cycles; Reich et al. (2008) demonstrate strong relationships between respiration and N scaling based on observational data from various species. At any normal N concentration, respiration rates are consistently lower on average in leaves than in stems or roots. Therefore, we introduce two parameters for stem and root, respectively, based on PFT to adjust the respiration rate in section 3.4.

Nitrogen also affects plant phenology and can be remobilized to supply spring bud-break or vegetative shoot extension (Kolb & Evans, 2002; Marmann et al., 1997; Millard, 1994; Neilsen et al., 1997). Nitrogen resorption is found during leaf senescence and growth in evergreens (May & Killingbeck, 1992). Because plants need time to turnover, the plant N processes also have a lag effect on plant phenology (Thomas et al., 2015). Phenology in SSiB4/TRIFFID modulates

LAI evolution, including leaf mortality, but it is not directly linked to N. Since different N states and supplements will lead to different lags on phenology, we add N impact on plant phenology by introducing a N limitation parameter and will be discussed in section 3.5.

3 The Development of SSiB5/TRIFFID/DayCent-SOM model

3.1 The SSiB5/TRIFFID/DayCent-SOM computational flow

In SSiB5/TRIFFID/DayCent-SOM, SSiB5 provides GPP, autotrophic respiration, and other physical variables such as canopy temperature and soil moisture every 3 hours for TRIFFID (Fig. 2). TRIFFID accumulates the GPP and respiration from SSiB5 and predicts biotic C, PFT fractional coverage, vegetation height, and LAI every ten days, which are used to update surface properties, such as albedo, roughness length, and aerodynamic/canopy resistances, in SSiB5. The plant C-N framework uses the meteorological forcings (i.e., air temperature and precipitation) and physical variables (i.e., soil moisture and soil temperature) provided by SSiB5 every 3 hours and the biophysical properties (vegetation fraction and biotic C) provided by TRIFFID, which is updated every ten days. The plant C-N interface framework calculates dynamic C/N ratios, N-limited photosynthesis, N-impacted respiration rate, and N-limited phenology every 3 hours. The C loss and potential N uptake are accumulated within one day in the C-N Interface Framework and plant C and N litter fall are transferred to DayCent-SOM at the end of the day. DayCent-SOM calculates inorganic N available for plant N uptake (N_{avail}) and N losses from nitrate leaching and N-trace gas emissions each day. TRIFFID updates the vegetation dynamics based on C balance on Day 10, using the NPP and PFT competition strategy. The updated vegetation dynamics are transferred to SSiB5 to reflect the N impact on the C cycle.

3.2 Dynamic C/N ratio based on plant growth and soil nitrogen storage

The N availability for new growth limits the C assimilation rate in plant through the C/N ratio, i.e., the model simulated NPP should be no more than $N_{\text{avail}} \times \text{C/N ratios}$. In the original TRIFFID parameterization, the C/N ratios for different plant components (leaf, root, and wood) are fixed based on plant functional types (Cox, 2001). In reality, changes in C/N ratios occur over the lifecycle of the plant and vary with nutrient availability, which are not captured in original SSiB4/TRIFFID models. Based on DayCent's method of determining variable C:N ratios for plants, a linear relationship between C/N ratio ($\text{CNR}_{\text{actual}}$) and N_{avail} is introduced to the SSiB5/TRIFFID/DayCent-SOM for each PFT's components (Fig 3, Eq 1).

$$\text{CNR}_{\text{actual}} = \begin{cases} \text{CNR}_{\text{max}}, & N_{\text{avail}} \geq N_{\text{demand.max}} \\ \text{CNR}_{\text{min}}, & N_{\text{avail}} \leq N_{\text{demand.min}} \end{cases} \quad \frac{N_{\text{avail}} - N_{\text{demand.max}}}{N_{\text{demand.min}} - N_{\text{demand.max}}} \times \text{CNR}_{\text{min}} + \frac{N_{\text{avail}} - N_{\text{demand.min}}}{N_{\text{demand.max}} - N_{\text{demand.min}}} \times \text{CNR}_{\text{max}} \quad N_{\text{demand.min}} < N_{\text{avail}} < N_{\text{demand.max}} \quad (1)$$

where N_{avail} is the amount of soil mineral nitrogen that was available at the end of the previous day (g N m^{-2}) calculated from DayCent-SOM. The minimum and maximum amounts of nitrogen required ($N_{\text{demand,min}}$, $N_{\text{demand,max}}$) for the potential NPP_p ($\text{g C m}^{-2} \text{ day}^{-1}$) that is obtained from SSiB4/TRIFFID are:

$$N_{\text{demand,min}} = \frac{\text{NPP}_p}{\text{CNR}_{\text{max}}} \quad (2)$$

$$N_{\text{demand,max}} = \frac{\text{NPP}_p}{\text{CNR}_{\text{min}}} \quad (3)$$

where CNR_{min} and CNR_{max} are the minimum and the maximum C/N ratio for each PFT's components (Table 1). This C:N ranges of leaves, fine roots, and stems/wood are from DayCent-SOM's user Manual, scientific basis, technical documentation and other published papers (Parton et al., 1993; Parton et al., 2007).

Since the DayCent-SOM only provide the total available nitrogen ($N_{\text{avail, total}}$) for the plant within one grid box, the nitrogen available for each PFT in the grid box and each component for each PFT is calculated as

$$N_{\text{avail}} = N_{\text{avail, total}} * \text{frac}_i * \sum_j \text{Cfrac}_{i,j} \quad (4)$$

where frac_i is the fraction of PFT i in one grid, and $\text{Cfrac}_{i,j}$ is the fraction of total $N_{\text{avail, total}}$ allocated to plant type i, component j, and is determined as

$$\text{Cfrac}_{i,j} = \frac{\text{Growth}_{i,j}}{\sum_j \text{Growth}_{i,j}} \quad (5)$$

where $\text{Growth}_{i,j}$ is the amount of new C allocated to plant type i, component j, and is calculated in TRIFFID.

The potential NPP_p that is allocated to each PFT's components is defined similarly as

$$\text{NPP}_p = \text{NPP}_i * \sum_j \text{Cfrac}_{i,j} \quad (6)$$

where NPP_i is the ith type's potential NPP and is calculated in TRIFFID.

3.3 Effect of nitrogen limitation on photosynthesis based on soil available nitrogen and plant C-N ratio

There are several different ways to represent N-limitation, including using N to scale down photosynthesis (Ghimire et al., 2016; Goll et al., 2017; Thum et al., 2019; Yu et al., 2020; Zaehle et al., 2015; Zhu et al., 2019), or potential gross primary productivity (GPP) to reflect N-availability (Gerber et al., 2010; Oleson et al., 2013; Wang et al., 2010), or defining an NPP cost of nitrogen uptake (Fisher et al., 2010). We choose the most physiological way, adjusting $V_{c,\text{max}}$ during the photosynthesis process, which regulates both C assimilation and autotrophic respiration, rather than net production (NPP) at the end of the photosynthesis process.

During photosynthesis the assimilation product, GPP, is proportional to the

maximum Rubisco carboxylation rate ($V_{c,\max}$) which is related to the N concentration.

We therefore introduce a downregulation of the canopy photosynthetic rate based on the available mineral N for new growth (N_{avail}) using a N-availability factor, $f(N)$.

$$V_{c,\max-\text{new}} = V_{c,\max} * f(N) \quad (7)$$

The $f(N)$ is determined by the nitrogen availability:

$$f(N) = \begin{cases} \frac{N_{\text{avail}}}{N_{\text{demand},\min}} & N_{\text{avail}} \leq N_{\text{demand},\min} \\ 1 & \text{otherwise} \end{cases} \quad (8)$$

Plants adjust the relative allocations of C and N during N uptake and via N remobilization and resorption to reduce the impact of N-limitation. We assume there is no N-limitation on photosynthesis when $N_{\text{avail}} > N_{\text{demand},\min}$. We add a linear relationship between $f(N)$ and N_{avail} when N availability is not sufficient for the minimum N demand for new growth. In this approach, a variable ($V_{c,\max}$), which is related to the N during the photosynthesis process and affects both C uptake and autotrophic respiration, is adjusted.

In fact, the factor, $f(N)$ can also be applied to NPP and GPP as shown in Equations 9a –b and had been done by the studies as reviewed at the beginning of this section.

$$NPP_{\text{new}} = NPP * f(N) \quad (9a)$$

$$GPP_{\text{new}} = GPP * f(N) \quad (9b)$$

If NPP is adjusted (Eq. 9a), this is equivalent to adding a photosynthesis N-limitation on plant respiration, which is not reasonable based on plant physiology and may distort the ration of NPP and respiration. In SSiB4/TRIFFID, GPP will be recalculated after determining the potential C achievement. We had tested all of these approaches and find that they all limit the end production (NPP) of the photosynthesis process, but adjusting $V_{c,\max}$ is the most direct and process-based one (See section 6.2 for more discussion).

3.4 Improvement of nitrogen impact on respiration rates based on field observations

Nitrogen affects plant respiration (Reich et al., 2008; Thornely & Johnson, 1990). In the original SSiB4/TRIFFID, the total maintenance respiration (R_{pm}) is given by Cox (2001):

$$R_{\text{pm}} = 0.012R_{\text{dc}} \frac{N_l + N_s + N_r}{N_l} \quad (10)$$

where R_{dc} is canopy dark respiration, N_l , N_s and N_r are the N contents of leaf, stem, and root, respectively, and the factor of 0.012 is from the unit conversion. Eq. (10) assumed the respiration rates in root and stem have the same dependence on N content as leaf. However, studies (Reich et al., 2008) had shown that

the respiration rates at any common N concentration were consistently lower in leaves than in stems or roots on average.

Thus, we introduce two PFT-specific parameters ($\text{Res}A_S$, $\text{Res}A_R$) from field observations (Wang et al., 2006; Yang et al., 1992) to represent root and stem respiration.

$$R_{\text{pm}} = 0.012R_{\text{dc}} \frac{N_l + \text{Res}A_S * N_s + \text{Res}A_R * N_r}{N_l} \quad (11)$$

Since $\text{Res}A_S$ and $\text{Res}A_R$ generally larger than 1, new R_{pm} is larger than the former one, the increased respiration due to the nitrogen limitation will decrease the NPP (= GPP – autotrophic respiration). Notably, the R_{dc} calculation linearly depends on $V_{c,\text{max}}$ thus the introduced N limitation of $V_{c,\text{max}}$ in section 3.3 may contradict the N effect on respiration.

3.5 N-limitation on LAI based on plant phenology

Studies (Aerts & Berendse, 1988; Thomas et al., 2015) show that leaf turnover and aboveground productivity are related to nutrient availability and that plant N processes can potentially lead to lags on phenology. In TRIFFID, a leaf phenology parameter, p , (Cox, 2001) is introduced to represent the vegetation’s phenological status, to calculate the leaf drop rate, and to adjust the model-simulated maximum possible LAI, which is based on carbon balance, LAI ($\text{LAI}_{\text{balance}}$), to actual LAI and produce realistic phenology.

$$\text{LAI} = p \times \text{LAI}_{\text{balance}} \quad (12)$$

and

$$\frac{dp}{dt} = \begin{cases} -\gamma_p & \gamma_{\text{lm}} > 2\gamma_0 \\ \gamma_p(1-p) & \gamma_{\text{lm}} \leq 2\gamma_0 \end{cases} \quad (13)$$

where leaf constant absolute drop rate $\gamma_p = 20 \text{ yr}^{-1}$, the leaf mortality rate γ_{lm} is a function of temperature T , and the minimum leaf turnover rate $\gamma_0 = 0.25$ (Cox, 2001). This phenology parameter, p , indicates that “full leaf” is approached asymptotically during the growing season, and p is reduced at a constant absolute rate when the mortality rate is larger than a threshold value. Otherwise, p increases but the rate of increase is reduced as the growing season evolves. To reflect the N limitation in SSiB5/TRIFFID/DayCent-SOM, we assume p , is limited by the N availability with the new p determined by

$$p_{\text{new}} = f(N) \times p_{\text{original}} \quad (14)$$

where $f(N)$ is calculated in section 3.3.

4. Preliminary evaluations using the measurements from three sites

This paper focuses on the impact of nitrogen process on the climatology of global carbon cycle. Most current DGVMs are mainly focused on long-term (decadal to thousands years or even long) simulations at global scale; the diurnal and seasonal variations are not a subject for their modelling. Moreover, such

long term in-situ measurements are also not available for comparison. However, since the SSiB5 is a process-based model, we take this advantage to make some preliminary evaluations with the site observation to provide additional evidence on model's performance with these short-term in-situ measurements. Three sites with representative biome types and climates zones were selected to evaluate the simulations of seasonal patterns of GPP over these sites (Table 3). They are CN-Dan site (Dangxiong in Tibetan plateau), which is located in the semi-arid area and covers C3-Grass; US-KS2 (Kennedy Space Center in US), which covers broadleaf deciduous trees, and BR-Sa1 (Santarem-Km67-Primary Forest in Amazon).

The simulation results are shown in Figure 4 and Table 4. Among three sites, the newly developed SSiB5 produces superior to that of SSiB4 at the CN-Dan site with more reasonable GPP variability. With the C-N plant framework, SSiB5 reduces the RMSE and bias in this site from 0.597 gC d^{-1} to 0.303 gC d^{-1} , and 0.873 gC d^{-1} to 0.516 gC d^{-1} , respectively. The standard deviation has also improved significantly. The simulations at the US-KS2 site also have some consistent but not substantial improvement as shown in the CN-Dan site. However, the results at the site BR-Sa1 are very similar between the SSiB5 and the SSiB4. We will further discuss the SSiB5 performance in the tropical rainforest in the following sections. The results indicate that after introducing a very complex N process, the model show improvements in two sites. Similar results in another site as well as in many other variables, such as surface fluxes (not shown). The tests in this section provide a glance for the model's performance after the development of SSiB5 in several sites with short-term data to gain preliminary confidence. The goal of this study focuses on model's performance on global carbon climatology. In the following sessions a set of long-term experiments are conducted to comprehensively investigate this subject.

5 Data and Experimental design for long-term simulation

5.1 data

5.1.1 Meteorological forcing data

The Princeton global meteorological dataset for land surface modeling (Sheffield et al., 2006) was used to drive SSiB4/TRIFFID from 1948 to 2007 at $1^\circ \times 1^\circ$ spatial resolution and 3-hourly temporal interval. This dataset, including surface air temperature, pressure, specific humidity, wind speed, downward short-wave radiation flux, downward long-wave radiation flux, and precipitation, was constructed by combining a suite of global observation-based datasets with the National Center for Environmental Prediction/National Center for Atmospheric Research reanalysis data.

5.1.2 Observational data

To access the climatological status, variation, and trends of simulated LAI, two widely used LAI products were used as references in this study: the Global Inventory Modeling and Mapping Studies (GIMMS) LAI and the Global LAnd

Surface Satellite (GLASS) LAI. GIMMS-LAI is based on the third generation of Normalized Difference Vegetation Index (NDVI3g) from the GIMMS group and an Artificial Neural Network model (Zhu et al., 2013). GIMMS-LAI provides a 1/12-degree resolution, 15-day composites, and spans July 1981 to December 2011. GLASS-LAI is generated from Advanced Very High Resolution Radiometer (AVHRR) (from 1982 to 1999 with 0.05-degree resolution) and MODIS (from 2000 to 2012 with 1 km resolution) reflectance data using general regression neural networks (Xiao et al., 2014). GIMMS and GLASS LAI, and the meteorological forcing data for overlap period 1982 to 2007, were remapped to 1-degree spatial resolution and a monthly temporal interval.

The Model Tree Ensemble (MTE) GPP product (Jung et al., 2009) was used as the reference to evaluate simulated GPP. MTE is based-on a machine learning technique in which the model is trained to predict the five C fluxes at FLUXNET sites driven by observed meteorological data, land cover data, and the remotely-sensed fraction of absorbed photosynthetic active radiation (Jung et al., 2009). The trained model was then applied at the grid-scale driven by gridded forcing data. MTE-GPP data was resampled to 1-degree spatial and a monthly temporal resolution. Please note, the MTE data does not include the CO₂ fertilization. We had a paper (Liu et al., 2019) discussing this issue. Since this effect mainly affect the trend, while this paper focuses on climatological mean and the difference between different experiments, the missing CO₂ fertilization in the FLUXNET-MTE should not affect our discussion too much.

5.2 Experimental design

5.2.1 Initial condition for equilibrium simulation

There are different ways to initialize the surface condition for the quasi-equilibrium simulation. Following previous SSiB4/TRIFFID study (Zhang et al., 2015), we set up the initial condition using the SSiB vegetation map and SSiB vegetation table, which are based on ground surveys and satellite-derived information (Dorman & Sellers, 1989; Xue et al., 2004; Zhang et al., 2015) with 100% occupation at each grid point for the dominant PFT and zero for other PFTs, then we ran the SSiB4/TRIFFID model with the climate forcing for 100 years to reach the equilibrium conditions. The vegetation and soil conditions then were used as the initial conditions for the subsequent model runs.

5.2.2 Control run and sensitivity runs

In this study, the SSiB4/TRIFFID was applied to produce the global vegetation distribution as the control run (Exp. SSiB4) then the control run was compared to model experimental simulations to assess the sensitivity of C cycle variability and trend to N processes. All the simulations are driven by real-forcing from 1948-2007 (Table 2). In the control run, using the quasi-equilibrium simulation results as the initial condition, SSiB4/TRIFFID is driven by the historical meteorological forcing from 1948 through 2007. Using the control simulation, we first evaluated the ability of the model to reproduce the climatology and variability of multiple biotic variables by comparing it to multiple observation-based

datasets. In addition to the control run, two sets of experiments were conducted to quantify the N process’s main effects on the C cycle. They were designed as follows:

- (1). Nitrogen limitation on photosynthesis (Exp. NIPSN): The same meteorological forcing used for the control (Exp. SSiB4) drives the model, but dynamic C/N ratios and N-limitation on $V_{c,max}$ (Eq. 7) are introduced. The difference between Exp. SSiB4 and Exp. NIPSN indicates the effect of N- limitation on photosynthesis.
- (2). SSiB5/TRIFFID/DayCent-SOM (Exp. SSiB5): The model was driven by the same meteorological forcing used for Exp. SSiB4, but all four N processes, i.e., dynamic C/N ratio, and N impacts on photosynthesis, autotrophic respiration, and phenology, are introduced. The difference between Exp. NIPSN and Exp. SSiB5 indicates the nitrogen effect on autotrophic respiration and phenology, and the difference between Exp. SSiB4 and Exp. SSiB5 indicates the effect of N dynamics.

Two additional sets of experiments were conducted to quantify the difference in the three N-limitation approach (Eq. 7, 9a, and 9b):

- (3). Nitrogen limitation on NPP (Exp. NINPP): The same meteorological forcing used for the control (Exp. SSiB4) drives the model, but dynamic C/N ratios and N-limitation on NPP are introduced (Eq. 9a). The difference between Exp. SSiB4 and Exp. NINPP indicates the effect of N- limitation on NPP.
- (4). Nitrogen limitation on GPP (Exp. NIGPP): The same meteorological forcing used for the control (Exp. SSiB4) drives the model, but dynamic C/N ratios and N-limitation on GPP are introduced (Eq. 9b). The difference between Exp. SSiB4 and Exp. NIGPP indicates the effect of N- limitation on GPP.

6 Results of long-term simulation

6.1 Evaluation of LAI and GPP at global level

The simulated GPP averaged over 1982-2007 is compared to FLUXNET-MTE GPP (Martin Jung et al., 2011) to examine the impact of model parameterization of N processes on C and ecosystem characteristics. Both SSiB4/TRIFFID (Exp. SSiB4) and SSiB5/TRIFFID/DayCent-SOM (Exp. SSiB5) capture the distribution of global GPP (Fig. 5). The highest GPP occurs in the tropical evergreen forest and decreases with latitude in both the observations and the model. However, Exp. SSiB4’s simulated GPP has a negative bias in the Amazon tropical forest and a positive bias in tropical Africa and boreal regions. This simulated global GPP is $1082.36 \text{ g C m}^{-2} \text{ yr}^{-1}$ (Table 5), higher than the estimate, $862.86 \text{ g C m}^{-2} \text{ yr}^{-1}$ in FLUXNET-MTE (Martin Jung et al., 2011). After introducing all N processes, Exp. SSiB5’s GPP prediction, $941.81 \text{ g C m}^{-2} \text{ yr}^{-1}$, is closer to observations compared to Exp. SSiB4, with a 16.3% improvement (Table 5). The correlation coefficients between observed and simulated monthly/annual mean GPPs are increased from 0.46/0.98 (Exp. SSiB4) to 0.50/0.99 (Exp. SSiB5), respectively (Fig. 7 and Fig. 8), showing the

improvement in simulation the seasonal cycle in SSiB5. The interannual variability in SSiB4 is very high (0.98). SSiB5 shows no substantial improvement. The GPP bias in tropical Africa and boreal regions is reduced, which shows an improvement in spatial simulation (the spatial correlation coefficient from 0.88 to 0.90, Fig. 5). Despite the general global improvement, the GPP simulation in the temperate East Asian mixed forest-grassland regions seems to get worse. SSiB4's simulation there is close to observations and the imposed N-limitation in SSiB5 increases the bias. This issue needs to be further investigated in the regions where the N-limitation is not dominant. Further improvements, such as better ecological understanding of plant N dynamics and plant N observations, are necessary in this regional research. In addition, the negative GPP bias in Amazon is increased. This issue will be discussed in section 6.3.

Exp. SSiB5 also improved predictions of LAI compared to the control (Fig. 6). The highest LAI occurs in the tropical evergreen forest and decreases with latitude in both the observations and the model. The simulated LAI in Exp. SSiB4 has a global positive bias. After introducing all nitrogen processes, the positive bias is reduced. Globally, Exp. SSiB5 has an LAI bias of 0.94/1.12 for GIMMS/GLASS, respectively (Table 6), which is lower than the LAI bias in Exp. SSiB4 (global bias = 1.26/1.44 for GIMMS/GLASS, respectively), with a 31.1% improvement (compared to GIMMS, Table 6). In addition, the correlation coefficients between observed and simulated monthly/annual average LAIs are improved from 0.49/0.97 (Exp. SSiB4) to 0.51/0.98 (Exp. SSiB5) (Fig. 7 and Fig. 8).

It is interesting to notice that despite the global general LAI reduction, the SSiB5 slightly increased LAI estimates in North Africa and India. The N-impacts on phenology and respiration cause a slight change in the vegetation from shrub (N. Africa) or C4 grass (India) to C3 grass in these areas. This contributes to the GPP and LAI increase (Fig. 11). In next sections, we will further identify the effect of N-limitation to each process, such as the photosynthesis process, on simulated GPP and LAI.

6.2 Effects of nitrogen limitation on photosynthesis

In this section, we discuss the results from Exp. NIPSN, which applies Eq. (7) to scale down the $V_{c,max}$. Exp. NIPSN has a lower global GPP bias (128.52 g C m⁻² yr⁻¹) compared to FLUXNET-MTE estimates than Exp. SSiB4 does (219.50 g C m⁻² yr⁻¹) (Fig. 9, Table 5). Exp. NIPSN has a global LAI bias of 1.13 (Fig. 10, Table 6), which is lower than the LAI bias in Exp. SSiB4 (1.26). The largest reductions in LAI bias are in the North American and Eurasian continents.

The highest GPP occurs in the tropical evergreen forest and decreases with latitude in Exp. SSiB4 and the other three model experiments (Exp. NIPSN, Exp. NINPP, Exp. NIGPP). However, compared to FLUXNET-MTE GPP (OBS), the simulated GPP in Exp. NIPSN has the lowest negative bias in the Amazon tropical forest and lowest positive bias in tropical Africa and boreal

regions (Fig. 9). Exp. NIPSN had lower global GPP bias ($128.52 \text{ g C m}^{-2} \text{ yr}^{-1}$, Fig. 9) compared to FLUXNET-MTE GPP estimates than Exp. NINPP ($173.38 \text{ g C m}^{-2} \text{ yr}^{-1}$) and Exp. NIGPP did ($154.31 \text{ g C m}^{-2} \text{ yr}^{-1}$). For global LAI, Exp. NIPSN had a bias of 1.13 (Fig. 10), which is lower than the LAI bias of Exp. NINPP (1.17) and Exp. NIGPP (1.15). The Exp. NIPSN approach yields the best results. This is because adjusting $V_{c,\max}$ is the most direct and process-based one on physiology, and the most suitable for SSiB5's model structure.

The simulated GPP in Exp. NIPSN (0.9020) has the larger spatial correlation coefficient with FLUXNET-MTE GPP than Exp. NINPP (0.8998) and Exp. NIGPP did (0.8900). For global LAI, Exp. NIPSN has a spatial correlation coefficient with GIMMS LAI of 0.8370 (Table 7), which is larger than the spatial correlation coefficient of Exp. NINPP (0.8340) and Exp. NIGPP (0.8246). The Exp. NIPSN approach yields the best results.

Exp. SSiB5 did not produce the best results everywhere. The Exp. SSiB5 GPP results had a greater negative bias than Exp. NIPSN in the temperate East Asian mixed forest-grassland area; however, the LAI results improved with SSiB5 for this region. As we address in section 6.1, this issue needs to be investigated with more data. By and large, Table 5 and Table 6 show two general things: after introducing N-limitation on photosynthesis, Exp. NIPSN reduces GPP and LAI compared to Exp. SSiB4. After introducing N-impacts on respiration and phenology, Exp. SSiB5 further reduces GPP and LAI compared to Exp. NIPSN in most regions. Since Exp. SSiB4 and Exp. NIPSN overestimate LAI in all areas, N-limitation helps Exp. SSiB5 to produce the best LAI results everywhere. However, SSiB4 doesn't overestimate in all regions. The introduced N-limitation does not guarantee Exp. SSiB5 produces the best results in every region. Since Exp. NIPSN did best at substantially reducing the biases of simulated GPP and LAI in SSiB5, we finally choose Eq. (7) rather than Eq. (9a) or (9b) to scale down the photosynthesis.

6.3 Attribution of N processes on C cycle

It is interesting to notice that despite the fact that N processes generally reduced the global GPP/LAI in our results, N-limitation on photosynthesis (indicated by Exp. NIPSN – Exp. SSiB4) and the other two N processes (N-impacts on phenology and respiration, indicated by Exp. SSiB5 – Exp. NIPSN) show different regional attributions (Fig. 11, Table 5 and Table 6). Because not only N but also P limitation constrain the magnitude of terrestrial C uptake in response to elevated carbon dioxide and climate change, efforts have been made to identify regions constrained by global nutrient limitation. Some studies (Lauenroth et al., 1978; Owensby et al., 1970) show that N is quite limiting to grassland plant production in temperate systems since 50% increases for dry grasslands and 100% increases for wet grasslands with N fertilizer additions. Du et al. (2020) examined global N and P limitation using the ratio of site-averaged leaf N and P resorption efficiencies of the dominant species across 171 sites, and found a strong latitudinal pattern of N and P limitation. N-

limitation prevails in boreal forests, tundra, temperate coniferous forests, and montane grasslands and shrublands, whereas phosphorus (P) has more effect in Mediterranean biomes, grasslands, savannas, shrublands and forests in tropical, subtropical and temperate regions.

The LAI and GPP bias reduction between Exp. SSiB4 and Exp. SSiB5 (Fig. 5f, Fig. 6f) as well as the experiments that examine the impact of N-limitation on different processes provide a global N-limitation pattern. Our simulations show a strong latitudinal pattern of N-limitation and relatively close agreement with Du et al. (2020) results but provide more comprehensive information. N-limitation on photosynthesis, which is shown in the difference between Exp. SSiB4 and Exp. NIPSN, results in a dominant decrease in tropical Africa and boreal regions (Fig. 11a), but N-impacts on phenology and respiration dominate the decline in GPP in tropical forests (Fig. 11b).

Moreover, there is a transition to N-limitation at higher elevations in some lower-latitude regions (i.e., the Tibetan Plateau) (Du et al., 2020). This pattern is also captured in this study (Fig.11a, Fig. 11c). It should be pointed out that using bias reduction of GPP/LAI to show N limitation pattern may not be sensitive to leaf N and P resorption efficiencies; however, it provides information on spatial heterogeneity and is a tool for comparing nutrient limitation globally to existing assessments based on site nutrient fertilization experiments. Since plant production in the Amazon area and Australia are typically P-limited, this may explain why SSiB5’s N-limitation is not very effective in these areas (Fig.11a, Fig. 11c). In the future we will need to add plant-soil P processes to consider both P and N limitation.

7 Discussion and Conclusions

This study presents improvements in modelling C cycle by introducing plant N processes into the SSiB5/TRIFFID/DayCent-SOM. We have employed DayCent-SOM to calculate the amount of N available to plants and plant soil N uptake, and have developed a plant C-N framework for modelling the C/N interactions. The new model structure in SSiB5/TRIFFID/DayCent-SOM allows us to use dynamic C/N ratios to represent plant resistance and self-adjustment. Since these processes can increase nutrient use efficiency and reduce the impact of nitrogen limitation through N remobilization and resorption, V_{max} is no longer in linear relation with leaf N content. This is a unique advantage of our model. That said, with the new SSiB5/TRIFFID/DayCent-SOM model structure, N impacts on GPP are predicted directly but not linearly with leaf N content, which is affected by the state of plant growth, autotrophic respiration, and plant phenology.

We systematically evaluated the model against multiple reference data sets for GPP, LAI, and global N-limitation patterns. In general, SSiB5/TRIFFID/DayCent-SOM has a lower bias for GPP and LAI than the baseline version of SSiB4/TRIFFID. The main improvements are found in tropical Africa and boreal forest, accompanied by a global decrease of the bias in GPP and

LAI by 16.3% and 27.1%, respectively. The more realistic representation of dynamic C/N ratios and plant N framework lead to general improvements in SSiB5/TRIFFID/DayCent-SOM's global C cycling predictions. From the perspective of plant physiology, the downregulation of the canopy photosynthetic rate based on the available mineral N for growth of plant tissues is more reasonable than the simple and direct downregulation of GPP or NPP. This coupled model can better reproduce observed state variables and their emergent properties (such as GPP, NPP, LAI, and respiration). The new model can also predict a global pattern of terrestrial N-limitation. It should be pointed out that the FLUXNET-MTE does not include CO₂ fertilization effect, but SSiB4 and SSiB5 both include. A study (Liu et al., 2019) has specifically investigate the fertilization effect. Since this effect mainly affect the trend, while this paper focuses on climatological mean and the difference between SSiB4 and SSiB5, the missing fertilization in the FLUXNET-MTE would not affect our discussion and conclusion too much.

Despite the general improvement globally, the GPP simulation in the temperate East Asian mixed forest-grassland regions seems to get worse. There are some regions with lower GPP than observations in SSiB4, the imposed N-limitation in SSiB5 would further increase the bias in the regions where the N-limitation is not dominant anymore. This mismatch is a common issue reported in a number of publications (Anav et al., 2015; Liu et al., 2019; Piao et al., 2013). Recently, the important influence of phosphorus availability on the terrestrial ecosystem carbon uptake has been increasingly realized. And the newly initiated ecosystem-scale manipulation experiments in phosphorus-poor environments (Fleischer et al., 2019) call for the need for new phosphorus enabled LSMs to keep track of these actions (Goll et al., 2017; Reed et al., 2015). This may also explain why SSiB5's N-limitation is not very effective in tropics (Fig.11a, Fig. 11c). We will incorporate other plant processes, such as plant/soil phosphorus processes, to improve the performance of model in the future.

Acknowledgments

This study is joint supported by the National Science Foundation, Division of Atmospheric and Geospace Sciences (Grant No. AGS-1419526, AGS-1849654), and the National Science Foundation of China (Grant No. 41775075). The authors acknowledge the use of the Cheyenne supercomputer (<https://doi.org/10.5065/D6RX99HX>, Computational and Information Systems Laboratory, 2019), provided by NCAR CISL, for providing HPC resources.

Author contributions. ZX, YX, MH, and YL designed the coupling strategy between SSiB4/TRIFFID and DayCent-SOM. ZX conducted the simulation with suggestions from YX, WB, and WG. ZX, YX, and MH drafted the text and ZX made the figures. All authors (ZX, YX, WG, MH, WG, PC, and YL) have contributed to the analysis and the text.

Data availability. The evaluation/reference data sets from model data discussed in this paper are archived at <https://doi.org/10.5281/zenodo.5126455>

References

- Aerts, R. (1996). Nutrient Resorption from Senescing Leaves of Perennials: Are there General Patterns? *The Journal of Ecology*, 84(4), 597. <https://doi.org/10.2307/2261481>
- Aerts, R., & Berendse, F. (1988). The effect of increased nutrient availability on vegetation dynamics in wet heathlands. *Vegetatio*, 76(1–2), 63–69. <https://doi.org/10.1007/BF00047389>
- Ali, A.A., Xu, C., Rogers, A., McDowell, N. G., Medlyn, B. E., Fisher, R. A., et al. (2015). Global-scale environmental control of plant photosynthetic capacity. *Ecological Applications*, 25(8), 2349–2365. <https://doi.org/10.1890/14-2111.1>
- Ali, Ashehad A., Xu, C., Rogers, A., McDowell, N. G., Medlyn, B. E., Fisher, R. A., et al. (2015). Global-scale environmental control of plant photosynthetic capacity. *Ecological Applications*, 25(8), 2349–2365. <https://doi.org/10.1890/14-2111.1>
- Anav, A., Friedlingstein, P., Beer, C., Ciais, P., Harper, A., Jones, C., et al. (2015). Spatiotemporal patterns of terrestrial gross primary production: A review. *Reviews of Geophysics*, 53(3), 785–818. <https://doi.org/10.1002/2015RG000483>
- Arora, V. K., Katavouta, A., Williams, R. G., Jones, C. D., Brovkin, V., Friedlingstein, P., et al. (2020). Carbon – concentration and carbon – climate feedbacks in CMIP6 models and their comparison to CMIP5 models, 4173–4222.
- Beer, C., Reichstein, M., Tomelleri, E., Ciais, P., Jung, M., Carvalhais, N., et al. (2010). Terrestrial Gross Carbon Dioxide Uptake: Global Distribution and Covariation with Climate. *Science*, 329(5993), 834–838. <https://doi.org/10.1126/science.1184984>
- Best, M. J., Pryor, M., Clark, D. B., Rooney, G. G., Essery, R. . L. H., Ménard, C. B., et al. (2011). The Joint UK Land Environment Simulator (JULES), model description – Part 1: Energy and water fluxes. *Geoscientific Model Development*, 4(3), 677–699. <https://doi.org/10.5194/gmd-4-677-2011>
- Bonan, G. B. (2008). Forests and Climate Change: Climate Benefits of Forests. *Science*, 320(June), 1444–1449.
- Bonan, Gordon B., Hartman, M. D., Parton, W. J., & Wieder, W. R. (2013). Evaluating litter decomposition in earth system models with long-term litterbag experiments: An example using the Community Land Model version 4 (CLM4). *Global Change Biology*, 19(3), 957–974. <https://doi.org/10.1111/gcb.12031>
- Clark, D. B., Mercado, L. M., Sitch, S., Jones, C. D., Gedney, N., Best, M. J., et al. (2011). The Joint UK Land Environment Simulator (JULES), model description – Part 2: Carbon fluxes and vegetation dynamics. *Geoscientific Model Development*, 4(3), 701–722. <https://doi.org/10.5194/gmd-4-701-2011>
- Clarkson, D. T., & Hanson, J. B. (1980). The Mineral Nutrition of Higher Plants. *Annual Review of Plant Physiology*, 31(1), 239–298. <https://doi.org/10.1146/annurev.pp.31.060180.001323>
- Collatz, G. J., Ball, J. T., Grivet, C., & Berry, J. A. (1991). Physiological and environmental regulation of stomatal conductance, photosynthesis and transpiration: a model that includes a laminar boundary layer. *Agricultural and Forest Meteorology*, 54(2–4), 107–136. [https://doi.org/10.1016/0168-1923\(91\)90002-8](https://doi.org/10.1016/0168-1923(91)90002-8)
- Cox, P. M. (2001). Description of the “TRIFFID” Dynamic Global Vegetation Model. *Hadley Centre Technical Note-24*.
- DAN, L., YANG, X., YANG, F.,

PENG, J., LI, Y., GAO, D., et al. (2020). Integration of nitrogen dynamics into the land surface model AVIM. Part 2: baseline data and variation of carbon and nitrogen fluxes in China. *Atmospheric and Oceanic Science Letters*, 13(6). <https://doi.org/10.1080/16742834.2020.1819145>

Davies-Barnard, T., Meyerholt, J., Zaehle, S., Friedlingstein, P., Brovkin, V., Fan, Y., et al. (2020). Nitrogen cycling in CMIP6 land surface models: Progress and limitations. *Biogeosciences*, 17(20), 5129–5148. <https://doi.org/10.5194/bg-17-5129-2020>

Dorman, J. L., & Sellers, P. J. (1989). A global climatology of albedo, roughness length and stomatal resistance for atmospheric general circulation models as represented by the Simple Biosphere Model (SiB). *Journal of Applied Meteorology*, 28(9), 833–855. [https://doi.org/10.1175/1520-0450\(1989\)028<0833:AGCOAR>2.0.CO;2](https://doi.org/10.1175/1520-0450(1989)028<0833:AGCOAR>2.0.CO;2)

Drewniak, B., & Gonzalez-Meler, M. (2017). Earth System Model Needs for Including the Interactive Representation of Nitrogen Deposition and Drought Effects on Forested Ecosystems. *Forests*, 8(8), 267. <https://doi.org/10.3390/f8080267>

Du, E., Terrer, C., Pellegrini, A. F. A., Ahlström, A., van Lissa, C. J., Zhao, X., et al. (2020). Global patterns of terrestrial nitrogen and phosphorus limitation. *Nature Geoscience*, 13(3), 221–226. <https://doi.org/10.1038/s41561-019-0530-4>

Evans, J. R. (1989). Photosynthesis and nitrogen relationships in leaves of C₃ plants. *Oecologia*, 78(1), 9–19. <https://doi.org/10.1007/BF00377192>

Eyring, V., Bony, S., Meehl, G. A., Senior, C. A., Stevens, B., Stouffer, R. J., & Taylor, K. E. (2016). Overview of the Coupled Model Intercomparison Project Phase 6 (CMIP6) experimental design and organization. *Geoscientific Model Development*, 9(5), 1937–1958. <https://doi.org/10.5194/gmd-9-1937-2016>

Farquhar, G. D., von Caemmerer, S., & Berry, J. A. (1980). A biochemical model of photosynthetic CO₂ assimilation in leaves of C₃ species. *Planta*, 149(1), 78–90. <https://doi.org/10.1007/BF00386231>

Fisher, J. B., Sitch, S., Malhi, Y., Fisher, R. A., Huntingford, C., & Tan, S.-Y. (2010). Carbon cost of plant nitrogen acquisition: A mechanistic, globally applicable model of plant nitrogen uptake, retranslocation, and fixation. *Global Biogeochemical Cycles*, 24(1), n/a–n/a. <https://doi.org/10.1029/2009gb003621>

Fleischer, K., Rammig, A., De Kauwe, M. G., Walker, A. P., Domingues, T. F., Fuchslueger, L., et al. (2019). Amazon forest response to CO₂ fertilization dependent on plant phosphorus acquisition. *Nature Geoscience*, 12(9). <https://doi.org/10.1038/s41561-019-0404-9>

Foley, J. A., Levis, S., Prentice, I. C., Pollard, D., & Thompson, S. L. (1998). Coupling dynamic models of climate and vegetation. *Global Change Biology*, 4(5), 561–579. <https://doi.org/10.1046/j.1365-2486.1998.t01-1-00168.x>

Friedlingstein, P., Cox, P., Betts, R., Bopp, L., von Bloh, W., Brovkin, V., et al. (2006). Climate–Carbon Cycle Feedback Analysis: Results from the C₄ MIP Model Intercomparison. *Journal of Climate*, 19(14), 3337–3353. <https://doi.org/10.1175/JCLI3800.1>

Gerber, S., Hedin, L. O., Oppenheimer, M., Pacala, S. W., & Shevliakova, E. (2010). Nitrogen cycling and feedbacks in a global dynamic land model. *Global Biogeochemical Cycles*, 24(1), 1–15. <https://doi.org/10.1029/2008GB003336>

Ghimire, B., Riley, W. J., Koven, C. D., Mu, M., & Randerson, J. T. (2016). Representing leaf and root physiological traits in CLM improves global carbon and nitrogen

cycling predictions. *Journal of Advances in Modeling Earth Systems*, 8(2), 598–613. <https://doi.org/10.1002/2015MS000538>Goll, D.S., Brovkin, V., Parida, B. R., Reick, C. H., Kattge, J., Reich, P. B., et al. (2012). Nutrient limitation reduces land carbon uptake in simulations with a model of combined carbon, nitrogen and phosphorus cycling. *Biogeosciences*, 9(9), 3547–3569. <https://doi.org/10.5194/bg-9-3547-2012>Goll, Daniel S., Winkler, A. J., Raddatz, T., Dong, N., Colin Prentice, I., Ciais, P., & Brovkin, V. (2017). Carbon-nitrogen interactions in idealized simulations with JS-BACH (version 3.10). *Geoscientific Model Development*, 10(5), 2009–2030. <https://doi.org/10.5194/gmd-10-2009-2017>Gregory, J. M., Jones, C. D., Cadule, P., & Friedlingstein, P. (2009). Quantifying carbon cycle feedbacks. *Journal of Climate*, 22(19), 5232–5250. <https://doi.org/10.1175/2009JCLI2949.1>Grosso, S. J. Del, Parton, W. J., Mosier, A. R., Ojima, D. S., Potter, C. S., Borken, W., et al. (2000). General CH₄ oxidation model and comparisons of CH₄ Oxidation in natural and managed systems. *Global Biogeochemical Cycles*, 14(4), 999–1019. <https://doi.org/10.1029/1999GB001226>Del Grosso, S. J., Parton, W. J., Mosier, A. R., Ojima, D. S., Kulmala, A. E., & Phongpan, S. (2000). General model for N₂O and N₂ gas emissions from soils due to denitrification. *Global Biogeochemical Cycles*, 14(4), 1045–1060. <https://doi.org/10.1029/1999GB001225>Del Grosso, S. J., Parton, W. J., Mosier, A. R., Holland, E. A., Pendall, E., Schimel, D. S., & Ojima, D. S. (2005). Modeling soil CO₂ emissions from ecosystems. *Biogeochemistry*, 73(1), 71–91. <https://doi.org/10.1007/s10533-004-0898-z>Harper, A. B., Cox, P. M., Friedlingstein, P., Wiltshire, A. J., Jones, C. D., Sitch, S., et al. (2016). Improved representation of plant functional types and physiology in the Joint UK Land Environment Simulator (JULES v4.2) using plant trait information. *Geoscientific Model Development*, 9(7), 2415–2440. <https://doi.org/10.5194/gmd-9-2415-2016>Herbert, D. A., & Fownes, J. H. (1999). Phosphorus limitation of forest leaf area and net primary production on a highly weathered soil. *Ecosystems*, 29(2), 242–25. <https://doi.org/10.1007/BF02186049>Hu, S., Chapin, F. S., Firestone, M. K., Field, C. B., & Chiariello, N. R. (2001). Nitrogen limitation of microbial decomposition in a grassland under elevated CO₂. *Nature*, 409(6817), 188–191. <https://doi.org/10.1038/35051576>Huang, H., Xue, Y., Li, F., & Liu, Y. (2020). Modeling long-term fire impact on ecosystem characteristics and surface energy using a process-based vegetation-fire model SSiB4/TRIFFID-Fire v1.0. *Geoscientific Model Development Discussions*, 1–41. <https://doi.org/10.5194/gmd-2020-122>Hungate, B. A., Dukes, J. S., Shaw, M. R., Luo, Y., & Field, C. B. (2003, November 28). Nitrogen and Climate Change. *Science*. <https://doi.org/10.1126/science.1091390>Jiang, L., Lu, L., Jiang, L., Qi, Y., & Yang, A. (2014). Impact of a detailed urban parameterization on modeling the urban heat island in Beijing using TEB-RAMS. *Advances in Meteorology*, 2014. <https://doi.org/10.1155/2014/602528>Jung, M., Reichstein, M., & Bondeau, A. (2009). Towards global empirical up-scaling of FLUXNET eddy covariance observations: Validation of a model tree ensemble approach using a biosphere model. *Biogeosciences*, 6(10), 2001–2013. <https://doi.org/10.5194/bg-6-2001-2009>Jung, Martin, Reichstein,

M., Margolis, H. A., Cescatti, A., Richardson, A. D., Arain, M. A., et al. (2011). Global patterns of land-atmosphere fluxes of carbon dioxide, latent heat, and sensible heat derived from eddy covariance, satellite, and meteorological observations. *Journal of Geophysical Research: Biogeosciences*, 116(3). <https://doi.org/10.1029/2010JG001566>Kattge, J., Knorr, W., Raddatz, T., & Wirth, C. (2009). Quantifying photosynthetic capacity and its relationship to leaf nitrogen content for global-scale terrestrial biosphere models. *Global Change Biology*, 15(4), 976–991. <https://doi.org/10.1111/j.1365-2486.2008.01744.x>Kolb, K. J., & Evans, R. D. (2002). Implications of leaf nitrogen recycling on the nitrogen isotope composition of deciduous plant tissues. *New Phytologist*, 156(1), 57–64. <https://doi.org/10.1046/j.1469-8137.2002.00490.x>Krinner, G., Viovy, N., de Noblet-Ducoudré, N., Ogée, J., Polcher, J., Friedlingstein, P., et al. (2005). A dynamic global vegetation model for studies of the coupled atmosphere-biosphere system. *Global Biogeochemical Cycles*, 19(1), 1–33. <https://doi.org/10.1029/2003GB002199>Lauenroth, W. K., Dodd, J. L., & Sims, P. L. (1978). The effects of water- and nitrogen-induced stresses on plant community structure in a semiarid grassland. *Oecologia*, 36(2). <https://doi.org/10.1007/BF00349810>Lawrence, D. M., Fisher, R. A., Koven, C. D., Oleson, K. W., Swenson, S. C., Bonan, G., et al. (2019). The Community Land Model Version 5: Description of New Features, Benchmarking, and Impact of Forcing Uncertainty. *Journal of Advances in Modeling Earth Systems*, 11(12), 4245–4287. <https://doi.org/10.1029/2018MS001583>LeBauer, D. S., & Treseder, K. K. (2008). NITROGEN LIMITATION OF NET PRIMARY PRODUCTIVITY IN TERRESTRIAL ECOSYSTEMS IS GLOBALLY DISTRIBUTED. *Ecology*, 89(2), 371–379. <https://doi.org/10.1890/06-2057.1>Liu, Y., Xue, Y., Macdonald, G., Cox, P., & Zhang, Z. (2019a). Global vegetation variability and its response to elevated CO₂, global warming, and climate variability - A study using the offline SSiB4/TRIFFID model and satellite data. *Earth System Dynamics*, 10(1), 9–29. <https://doi.org/10.5194/esd-10-9-2019Ma>, H.-Y., Mechoso, C. R., Xue, Y., Xiao, H., Neelin, J. D., & Ji, X. (2013). On the connection between continental-scale land surface processes and the tropical climate in a coupled ocean-atmosphere-land system. *Journal of Climate*, 26(22), 9006–9025. <https://doi.org/10.1175/JCLI-D-12-00819.1>Makino, A., & Osmond, B. (1991). Effects of Nitrogen Nutrition on Nitrogen Partitioning between Chloroplasts and Mitochondria in Pea and Wheat. *Plant Physiology*, 96(2), 355–362. <https://doi.org/10.1104/pp.96.2.355>Marmann, P., Wendler, R., Millard, P., & Heilmeyer, H. (1997). Nitrogen storage and remobilization in ash (*Fraxinus excelsior*) under field and laboratory conditions. *Trees - Structure and Function*, 11(5), 298–305. <https://doi.org/10.1007/s004680050088>Matson, P., Lohse, K. A., & Hall, S. J. (2002). The Globalization of Nitrogen Deposition: Consequences for Terrestrial Ecosystems. *AMBIO: A Journal of the Human Environment*, 31(2), 113–119. <https://doi.org/10.1579/0044-7447-31.2.113>May, J. D., & Killingbeck, K. T. (1992). Effects of preventing nutrient resorption on plant fitness and foliar nutrient dynamics. *Ecology*, 73(5), 1868–1878. <https://doi.org/10.2307/1940038>Medlyn, B. E., Zaehle, S., De Kauwe, M. G., Walker, A. P., Dietze, M. C., Hanson, P. J., et al. (2015). Using ecosystem ex-

periments to improve vegetation models. *Nature Climate Change*, 5(6), 528–534. <https://doi.org/10.1038/nclimate2621>

Millard, P. (1994). Measurement of the remobilization of nitrogen for spring leaf growth of trees under field conditions. *Tree Physiology*, 14(7–9), 1049–1054. <https://doi.org/10.1093/treephys/14.7-8-9.1049>

Neilsen, D., Millard, P., Neilsen, G. H., & Hogue, E. J. (1997). Sources of N for leaf growth in a high-density apple (*Malus domestica*) orchard irrigated with ammonium nitrate solution. *Tree Physiology*, 17(11), 733–739. <https://doi.org/10.1093/treephys/17.11.733>

Niu, G. Y., Fang, Y. H., Chang, L. L., Jin, J., Yuan, H., & Zeng, X. (2020). Enhancing the Noah-MP Ecosystem Response to Droughts With an Explicit Representation of Plant Water Storage Supplied by Dynamic Root Water Uptake. *Journal of Advances in Modeling Earth Systems*, 12(11). <https://doi.org/10.1029/2020MS002062>

Oleson, K. W., Lawrence, D. M., Bonan, G. B., Drewniak, B., Huang, M., Charles, D., et al. (2013). Technical description of version 4.5 of the Community Land Model (CLM), NCAR Technical Note NCAR/TN-503+STR., National Center for Atmospheric Research, Boulder, CO, (July), 420pp. <https://doi.org/DOI:10.5065/D6RR1W7M>

Owensby, C. E., Hyde, R. M., & Anderson, K. L. (1970). Effects of Clipping and Supplemental Nitrogen and Water on Loamy Upland Bluestem Range. *Journal of Range Management*, 23(5). <https://doi.org/10.2307/3896163>

Pan, Y., Liu, Y., Wentworth, G. R., Zhang, L., Zhao, Y., Li, Y., et al. (2017). Letter to the editor: Critical assessments of the current state of scientific knowledge, terminology, and research needs concerning the ecological effects of elevated atmospheric nitrogen deposition in China. *Atmospheric Environment*, 153, 109–116. <https://doi.org/10.1016/j.atmosenv.2017.01.015>

Parton, W. J., Stewart, J. W. B., & Cole, C. V. (1988). Dynamics of C, N, P and S in grassland soils: a model. *Biogeochemistry*, 5(1), 109–131. <https://doi.org/10.1007/BF02180320>

Parton, W. J., Ojima, D. S., Cole, C. V., & Schimel, D. S. (1994). A general model for soil organic matter dynamics: sensitivity to litter chemistry, texture and management. *Quantitative Modeling of Soil Forming Processes. Proc. Symposium, Minneapolis, 1992*.

Parton, W. J., Scurlock, J. M. O., Ojima, D. S., Gilmanov, T. G., Scholes, R. J., Schimel, D. S., et al. (1993). Observations and modeling of biomass and soil organic matter dynamics for the grassland biome worldwide. *Global Biogeochemical Cycles*, 7(4), 785–809. <https://doi.org/10.1029/93GB02042>

Parton, William J., Hanson, P. J., Swanston, C., Torn, M., Trumbore, S. E., Riley, W., & Kelly, R. (2010). ForCent model development and testing using the Enriched Background Isotope Study experiment. *Journal of Geophysical Research: Biogeosciences*, 115(4), 1–15. <https://doi.org/10.1029/2009JG001193>

Parton, William J., Hartman, M., Ojima, D., & Schimel, D. (1998). DAYCENT and its land surface submodel: description and testing. *Global and Planetary Change*, 19(1–4), 35–48. [https://doi.org/10.1016/S0921-8181\(98\)00040-X](https://doi.org/10.1016/S0921-8181(98)00040-X)

Pastorello, G., Trotta, C., Canfora, E., Chu, H., Christianson, D., Cheah, Y. W., et al. (2020). The FLUXNET2015 dataset and the ONEFlux processing pipeline for eddy covariance data. *Scientific Data*, 7(1). <https://doi.org/10.1038/s41597-020-0534-3>

Peñuelas, J., Poulter, B., Sardans, J., Ciais, P., Van Der Velde, M.,

Bopp, L., et al. (2013). Human-induced nitrogen-phosphorus imbalances alter natural and managed ecosystems across the globe. *Nature Communications*, 4. <https://doi.org/10.1038/ncomms3934>Piao, S., Sitch, S., Ciais, P., Friedlingstein, P., Peylin, P., Wang, X., et al. (2013). Evaluation of terrestrial carbon cycle models for their response to climate variability and to CO₂ trends. *Global Change Biology*, 19(7), 2117–2132. <https://doi.org/10.1111/gcb.12187>Raddatz, T. J., Reick, C. H., Knorr, W., Kattge, J., Roeckner, E., Schnur, R., et al. (2007). Will the tropical land biosphere dominate the climate-carbon cycle feedback during the twenty-first century? *Climate Dynamics*, 29(6), 565–574. <https://doi.org/10.1007/s00382-007-0247-8>Reed, S. C., Yang, X., & Thornton, P. E. (2015). Incorporating phosphorus cycling into global modeling efforts: A worthwhile, tractable endeavor. *New Phytologist*, 208(2). <https://doi.org/10.1111/nph.13521>Reich, P. B., Hobbie, S. E., Lee, T., Ellsworth, D. S., West, J. B., Tilman, D., et al. (2006). Nitrogen limitation constrains sustainability of ecosystem response to CO₂. *Nature*, 440(7086), 922–925. <https://doi.org/10.1038/nature04486>Reich, P. B., Tjoelker, M. G., Pregitzer, K. S., Wright, I. J., Oleksyn, J., & Machado, J. L. (2008). Scaling of respiration to nitrogen in leaves, stems and roots of higher land plants. *Ecology Letters*, 11(8), 793–801. <https://doi.org/10.1111/j.1461-0248.2008.01185.x>Richardson, A. D., Anderson, R. S., Arain, M. A., Barr, A. G., Bohrer, G., Chen, G., et al. (2012). Terrestrial biosphere models need better representation of vegetation phenology: Results from the North American Carbon Program Site Synthesis. *Global Change Biology*, 18(2). <https://doi.org/10.1111/j.1365-2486.2011.02562.x>Rogers, A. (2014). The use and misuse of V(c,max) in Earth System Models. *Photosynthesis Research*, 119(1–2), 15–29. <https://doi.org/10.1007/s11120-013-9818-1>Sellers, P. J., Mintz, Y., Sud, Y. C., & Dalcher, A. (1986). A Simple Biosphere Model (SIB) for Use within General Circulation Models. *Journal of the Atmospheric Sciences*, 43(6), 505–531. [https://doi.org/10.1175/1520-0469\(1986\)043<0505:ASBMFU>2.0.CO;2](https://doi.org/10.1175/1520-0469(1986)043<0505:ASBMFU>2.0.CO;2)Sheffield, J., Goteti, G., & Wood, E. F. (2006). Development of a 50-year high-resolution global dataset of meteorological forcings for land surface modeling. *Journal of Climate*, 19(13), 3088–3111. <https://doi.org/10.1175/JCLI3790.1>Sitch, S., Smith, B., Prentice, I. C., Arneth, A., Bondeau, A., Cramer, W., et al. (2003). Evaluation of ecosystem dynamics, plant geography and terrestrial carbon cycling in the LPJ dynamic global vegetation model. *Global Change Biology*, 9(2), 161–185. <https://doi.org/10.1046/j.1365-2486.2003.00569.x>Smith, B., Wärlind, D., Arneth, A., Hickler, T., Leadley, P., Siltberg, J., & Zaehle, S. (2014). Implications of incorporating N cycling and N limitations on primary production in an individual-based dynamic vegetation model. *Biogeosciences*, 11(7), 2027–2054. <https://doi.org/10.5194/bg-11-2027-2014>Talhelm, A. F., Pregitzer, K. S., & Burton, A. J. (2011). No evidence that chronic nitrogen additions increase photosynthesis in mature sugar maple forests. *Ecological Applications*, 21(7), 2413–2424. <https://doi.org/10.1890/10-2076.1>Thomas, R. Q., Brookshire, E. N. J., & Gerber, S. (2015). Nitrogen limitation on land: How can it occur in Earth system models? *Global Change Biology*, 21(5), 1777–1793.

<https://doi.org/10.1111/gcb.12813>Thornely, J. H. M., & Johnson, I. R. (1990). Plant Growth Modelling: A Mathematical approach to Plant and Crop Physiology. Thornton, P. E., Lamarque, J.-F., Rosenbloom, N. A., & Mahowald, N. M. (2007). Influence of carbon-nitrogen cycle coupling on land model response to CO₂ fertilization and climate variability. *Global Biogeochemical Cycles*, 21(4). <https://doi.org/10.1029/2006GB002868>Thornton, P. E., Doney, S. C., Lindsay, K., Moore, J. K., Mahowald, N., Randerson, J. T., et al. (2009). Carbon-nitrogen interactions regulate climate-carbon cycle feedbacks: Results from an atmosphere-ocean general circulation model. *Biogeosciences*, 6(10), 2099–2120. <https://doi.org/10.5194/bg-6-2099-2009>Thum, T., Caldararu, S., Engel, J., Kern, M., Pallandt, M., Schnur, R., et al. (2019). A new model of the coupled carbon, nitrogen, and phosphorus cycles in the terrestrial biosphere (QUINCY v1.0; revision 1996). *Geoscientific Model Development*, 12(11). <https://doi.org/10.5194/gmd-12-4781-2019>Vicca, S., Luyssaert, S., Peñuelas, J., Campioli, M., Chapin, F. S., Ciais, P., et al. (2012). Fertile forests produce biomass more efficiently. *Ecology Letters*, 15(6), 520–526. <https://doi.org/10.1111/j.1461-0248.2012.01775.x>Vitousek, Peter. (1982). Nutrient Cycling and Nutrient Use Efficiency Author (s): Peter Vitousek Source: The American Naturalist, Vol. 119, No. 4 (Apr., 1982), pp. 553–572 Published by: The University of Chicago Press for The American Society of Naturalists Stable URL, 119(4), 553–572.Vitousek, PeterM., & Howarth, R. (1991). Nitrogen limitation on land and in the sea: How can it occur? *Biogeochemistry*, 13(2), 3646–3653. <https://doi.org/10.1007/BF00002772>Wang, Y. P., Law, R. M., & Pak, B. (2010a). A global model of carbon, nitrogen and phosphorus cycles for the terrestrial biosphere. *Biogeosciences*, 7(7), 2261–2282. <https://doi.org/10.5194/bg-7-2261-2010>Wiltshire, A., Burke, E., Chadburn, S., Jones, C., Cox, P., Davies-Barnard, T., et al. (2020). JULES-CN: a coupled terrestrial Carbon-Nitrogen Scheme (JULES vn5.1). *Geoscientific Model Development Discussions*, (July), 1–40. <https://doi.org/10.5194/gmd-2020-205>Xiao, Z., Liang, S., Wang, J., Chen, P., Yin, X., Zhang, L., & Song, J. (2014). Use of general regression neural networks for generating the GLASS leaf area index product from time-series MODIS surface reflectance. *IEEE Transactions on Geoscience and Remote Sensing*, 52(1), 209–223. <https://doi.org/10.1109/TGRS.2013.2237780>Xue, Y., Sellers, P. J., Kinter, J. L., & Shukla, J. (1991). A Simplified biosphere model for global climate studies. *Journal of Climate*. [https://doi.org/10.1175/1520-0442\(1991\)004<0345:ASBMFG>2.0.CO;2](https://doi.org/10.1175/1520-0442(1991)004<0345:ASBMFG>2.0.CO;2)Xue, Y., Juang, H.-M. H., Li, W.-P., Prince, S., DeFries, R., Jiao, Y., & Vasic, R. (2004). Role of land surface processes in monsoon development: East Asia and West Africa. *Journal of Geophysical Research D: Atmospheres*, 109(3).Xue, Y., De Sales, F., Vasic, R., Mechoso, C. R., Arakawa, A., & Prince, S. (2010). Global and seasonal assessment of interactions between climate and vegetation biophysical processes: A GCM study with different land-vegetation representations. *Journal of Climate*, 23(6), 1411–1433. <https://doi.org/10.1175/2009JCLI3054.1>Yang, X., Dan, L., Yang, F., Peng, J., Li, Y., Gao, D., et al. (2019). The integration of nitrogen dynamics into a land surface model. Part 1: model description

and site-scale validation. *Atmospheric and Oceanic Science Letters*, 12(1). <https://doi.org/10.1080/16742834.2019.1548246>

Yu, L., Ahrens, B., Wutzler, T., Zaehle, S., & Schrumpf, M. (2020). Modeling Soil Responses to Nitrogen and Phosphorus Fertilization Along a Soil Phosphorus Stock Gradient. *Frontiers in Forests and Global Change*, 3. <https://doi.org/10.3389/ffgc.2020.543112>

Zaehle, S., Jones, C. D., Houlton, B., Lamarque, J.-F., & Robertson, E. (2015). Nitrogen availability reduces CMIP5 projections of twenty-first-century land carbon uptake. *Journal of Climate*, 28(6), 2494–2511. <https://doi.org/10.1175/JCLI-D-13-00776.1>

Zhan, X., Xue, Y., & Collatz, G. J. (2003). An analytical approach for estimating CO₂ and heat fluxes over the Amazonian region. *Ecological Modelling*, 162(1–2), 97–117. [https://doi.org/10.1016/S0304-3800\(02\)00405-2](https://doi.org/10.1016/S0304-3800(02)00405-2)

Zhang, Z., Xue, Y., MacDonald, G., Cox, P. M., & Collatz, G. J. (2015). Investigation of North American vegetation variability under recent climate: A study using the SSiB4/TRIFFID biophysical/dynamic vegetation model. *Journal of Geophysical Research*, 120(4), 1300–1321. <https://doi.org/10.1002/2014JD021963>

Zhu, Q., Riley, W. J., Tang, J., Collier, N., Hoffman, F. M., Yang, X., & Bisht, G. (2019). Representing Nitrogen, Phosphorus, and Carbon Interactions in the E3SM Land Model: Development and Global Benchmarking. *Journal of Advances in Modeling Earth Systems*, 11(7). <https://doi.org/10.1029/2018MS001571>

Zhu, Z., Bi, J., Pan, Y., Ganguly, S., Anav, A., Xu, L., et al. (2013). Global data sets of vegetation leaf area index (LAI)_{3g} and fraction of photosynthetically active radiation (FPAR)_{3g} derived from global inventory modeling and mapping studies (GIMMS) normalized difference vegetation index (NDVI_{3G}) for the period 1981 to 2000. *Remote Sensing*, 5(2), 927–948. <https://doi.org/10.3390/rs5020927>

Table 1. C:N ranges (CNR) of leaves, fine roots, and stems/wood for each plant function type (PFT).

(*CNR_{min}* and *CNR_{max}* are the minimum and the maximum C/N ratio for each PFT's components. Data are from DayCent-SOM's user manual and other publications (Parton et al., 1993; Parton et al., 2007))

| PFT | Plant part | C:N Minimum | C:N Maximum |
|----------------------|------------|-------------|-------------|
| Broadleaf deciduous | leaves | 20 | 50 |
| | roots | 40 | 70 |
| | wood | 200 | 500 |
| Broadleaf Evergreen | leaves | 20 | 40 |
| | roots | 40 | 70 |
| | wood | 150 | 300 |
| Needleleaf Evergreen | leaves | 30 | 60 |
| | roots | 40 | 60 |
| | wood | 400 | 800 |
| C3 grass | leaves | 20 | 40 |
| | roots | 40 | 50 |
| | wood | 40 | 80 |
| C4 grass | leaves | 20 | 60 |
| | roots | 60 | 100 |
| | wood | 60 | 100 |
| shrub | leaves | 20 | 40 |
| | roots | 40 | 70 |
| | wood | 200 | 400 |
| tundra shrub | leaves | 20 | 40 |
| | roots | 40 | 80 |
| | wood | 300 | 700 |

Table 2. Experimental design


| | | |
|----------------------------------|--|---|
| 100-year equilibrium | <i>Initial condition</i>  | Real-forcing simulation 1948-2007 |
| <i>Fixed climatology forcing</i> | | <i>Transient forcing</i> |
| Control experiment | | SSiB4: Control experiment DIPSN: Nitrogen limitation on p hotosynthesis(V max) DINPP: Nitrogen limitation on photosynthesis(NPP) DIGPP: Nitrogen limitation on photosynthesis(GPP) SSiB5: including all four nitrogen processes |

Table 3 The information of FLUXNET sites used for model validation

| Site ID | Site name | LAT | LONG | PFT | Time |
|---------|----------------------------------|-------|--------|---------------------|-----------|
| CN-Dan | Dangxiong | 30.50 | 91.07 | C3 grass | 2004-2005 |
| US-KS2 | Kennedy Space Center (scrub oak) | 28.61 | -80.67 | Broadleaf deciduous | 2003-2006 |
| BR-Sa1 | Santarem-Km67-Primary Forest | -2.86 | -54.96 | Broadleaf Evergreen | 2002-2011 |

Table 4. The intercomparisons of bias, standard deviation and RMSE between SSiB4 and SSiB5 over three sites.

| Site_ID | Bias (gC d ⁻¹) | | Standard deviation (gC d ⁻¹) | | | RMSE (gC d ⁻¹) | |
|---------|----------------------------|--------|--|-------|-------|----------------------------|-------|
| | SSiB4 | SSiB5 | OBS | SSiB4 | SSiB5 | SSiB4 | SSiB5 |
| CN-Dan | 0.873 | 0.516 | 0.949 | 1.485 | 1.071 | 0.60 | 0.30 |
| US-KS2 | 0.125 | -0.033 | 1.391 | 1.574 | 1.543 | 3.92 | 3.72 |
| BR-Sa1 | 0.040 | 0.036 | 1.550 | 1.241 | 1.241 | 3.01 | 3.00 |

Table 5. Regional and Global GPP for (a) FLUXNET-MTE GPP, (b) SSiB4 (control), (c) NIPSN (N limitation on photosynthesis only) and (d) SSiB5 (N limitation on photosynthesis, autotrophic respiration, and phenology).

| Regions | Sub-regions | GPP Mean (gC m ⁻² yr ⁻¹) | | | | | | | |
|-----------------------------------|----------------------|---|------|-------------|-------------------|------------|-------------------|------------|-----------------|
| | | MTE | | SSiB4 | | NIPSN | | SSiB5 | |
| | | mean | bias | mean | bias | mean | bias | mean | bias |
| Arid and Semi-Arid Areas | West Africa | 893 | | 1147 | 254(28.5%) | 963 | 70(7.9%) | 915 | 22(2.5%) |
| | West NA | 438 | | 549 | 111(25.4%) | 454 | 16(3.5%) | 431 | -7(-1.6%) |
| | SA Savanna | 1665 | | 1860 | 195(11.7%) | 1763 | 98(5.9%) | 1675 | 10(0.6%) |
| | East Africa | 1228 | | 1533 | 306(24.9%) | 1427 | 199(16.2%) | 1356 | 128(10.4%) |
| | East Asian semi-arid | 1440 | | 1470 | 30(2.1%) | 1199 | -241(-16.7%) | 1139 | -301(-20.9%) |
| NH High-Mid Latitude Areas | NA High-Mid Latitude | 552 | | 814 | 262(47.6%) | 700 | 149(27.0%) | 665 | 114(20.6%) |
| | Eurasian High-Mid | 844 | | 966 | 122(14.5%) | 871 | 27(3.2%) | 827 | 16(-2.0%) |
| Equator | Amazon Basin | 2993 | | 2668 | -326(-10.9%) | 2631 | -362(-12.1%) | 2500 | -494(-16.5%) |
| | Southeast Asia | 2778 | | 2540 | -238(-8.6%) | 2419 | -359(-12.9%) | 2298 | -480(-17.3%) |
| | Equator Africa | 2522 | | 2645 | 123(4.9%) | 2611 | 89(3.5%) | 2481 | -42(-1.7%) |
| Subarctic Areas and Tibet | NA Subarctic | 234 | | 364 | 130(55.7%) | 240 | 6(2.4%) | 228 | -6(-2.7%) |
| | Eurasian Subarctic | 331 | | 484 | 153(46.2%) | 328 | -3(-1.0%) | 311 | -20(-6.0%) |
| | Tibet | 409 | | 561 | 153(37.3%) | 298 | -111(-27.2%) | 283 | 126(-30.8%) |
| Global | | 863 | | 1082 | 220(25.4%) | 991 | 129(14.9%) | 942 | 79(9.1%) |

Note: the numbers in parentheses are relative biases

Table 6. Same as Table 5, but for LAI.

| Regions | Sub-regions | LAI Mean (m ² m ⁻²) | | | | | | | | | |
|----------------------------|----------------------|--|------|-------|---------------|-------|--------------|-------|-------------|-------|-------------|
| | | GIMMS | | GLASS | | SSiB4 | | NIPSN | | SSiB5 | |
| | | mean | bias | mean | bias | mean | bias | mean | bias | mean | bias |
| Arid and Semi-Arid Areas | West Africa | 1.08 | | 1.01 | -0.07(-6.5%) | 2.04 | 0.96(88.9%) | 1.89 | 0.81(75.0%) | 1.73 | 0.65(60.2%) |
| | West NA | 0.62 | | 0.49 | -0.13(-21.0%) | 1.38 | 0.76(122.6%) | 1.18 | 0.56(90.3%) | 1.09 | 0.47(75.8%) |
| | SA Savanna | 1.99 | | 1.91 | -0.18(-4.0%) | 3.34 | 1.35(67.8%) | 3.23 | 1.24(62.3%) | 2.97 | 0.98(49.2%) |
| | East Africa | 1.59 | | 1.55 | -0.04(-2.5%) | 3.02 | 1.43(89.9%) | 2.89 | 1.30(81.8%) | 2.66 | 1.07(67.3%) |
| | East Asian semi-arid | 1.60 | | 1.36 | -0.24(-15.0%) | 3.35 | 1.75(109.4%) | 2.84 | 1.24(77.5%) | 2.61 | 1.01(63.1%) |
| NH High-Mid Latitude Areas | NA High-Mid Latitude | 0.84 | | 0.49 | -0.35(-41.7%) | 1.91 | 1.07(127.4%) | 1.66 | 0.82(97.6%) | 1.53 | 0.69(82.1%) |
| | Eurasian High-Mid | 1.14 | | 0.57 | -0.57(-50.0%) | 2.29 | 1.15(100.9%) | 2.08 | 0.94(82.5%) | 1.91 | 0.77(67.5%) |
| Equator | Amazon Basin | 4.19 | | 4.08 | -0.11(-2.6%) | 6.01 | 1.82(43.4%) | 5.98 | 1.79(42.7%) | 5.50 | 1.31(31.3%) |
| | Southeast Asia | 3.93 | | 3.88 | -0.05(-1.3%) | 4.68 | 0.75(19.1%) | 4.68 | 0.75(19.1%) | 4.31 | 0.38(9.7%) |
| | Equator Africa | 3.83 | | 3.76 | -0.07(-1.8%) | 5.74 | 1.91(49.9%) | 5.72 | 1.89(49.3%) | 5.27 | 1.44(37.6%) |
| Subarctic Areas and Tibet | NA Subarctic | 0.32 | | 0.14 | -0.18(-56.3%) | 0.71 | 0.39(121.9%) | 0.51 | 0.19(59.4%) | 0.47 | 0.15(46.9%) |
| | Eurasian Subarctic | 0.33 | | 0.12 | -0.21(-63.6%) | 0.87 | 0.54(163.6%) | 0.65 | 0.32(97.0%) | 0.60 | 0.27(81.8%) |
| | Tibet | 0.64 | | 0.54 | -0.10(-15.6%) | 1.36 | 0.72(112.5%) | 0.81 | 0.17(26.6%) | 0.75 | 0.11(17.2%) |
| Global | | 1.18 | | 1.00 | -0.18(-15.3%) | 2.44 | 1.26(110.8%) | 2.31 | 1.13(95.8%) | 2.12 | 0.94(79.7%) |

Note: the numbers in parentheses are relative biases.

Table 7. The spatial correlation coefficient (SCC) between model simulations and OBS.

| LAI SCC | NIPSN | NINPP | NI GPP |
|----------------|----------|----------|----------|
| OBS | 0.8370** | 0.8340** | 0.8246** |
| GPP SCC | NIPSN | NINPP | NI GPP |
| OBS | 0.9020** | 0.8998** | 0.8900** |

Note: ** indicates correlation is significant at $p < 0.01$.

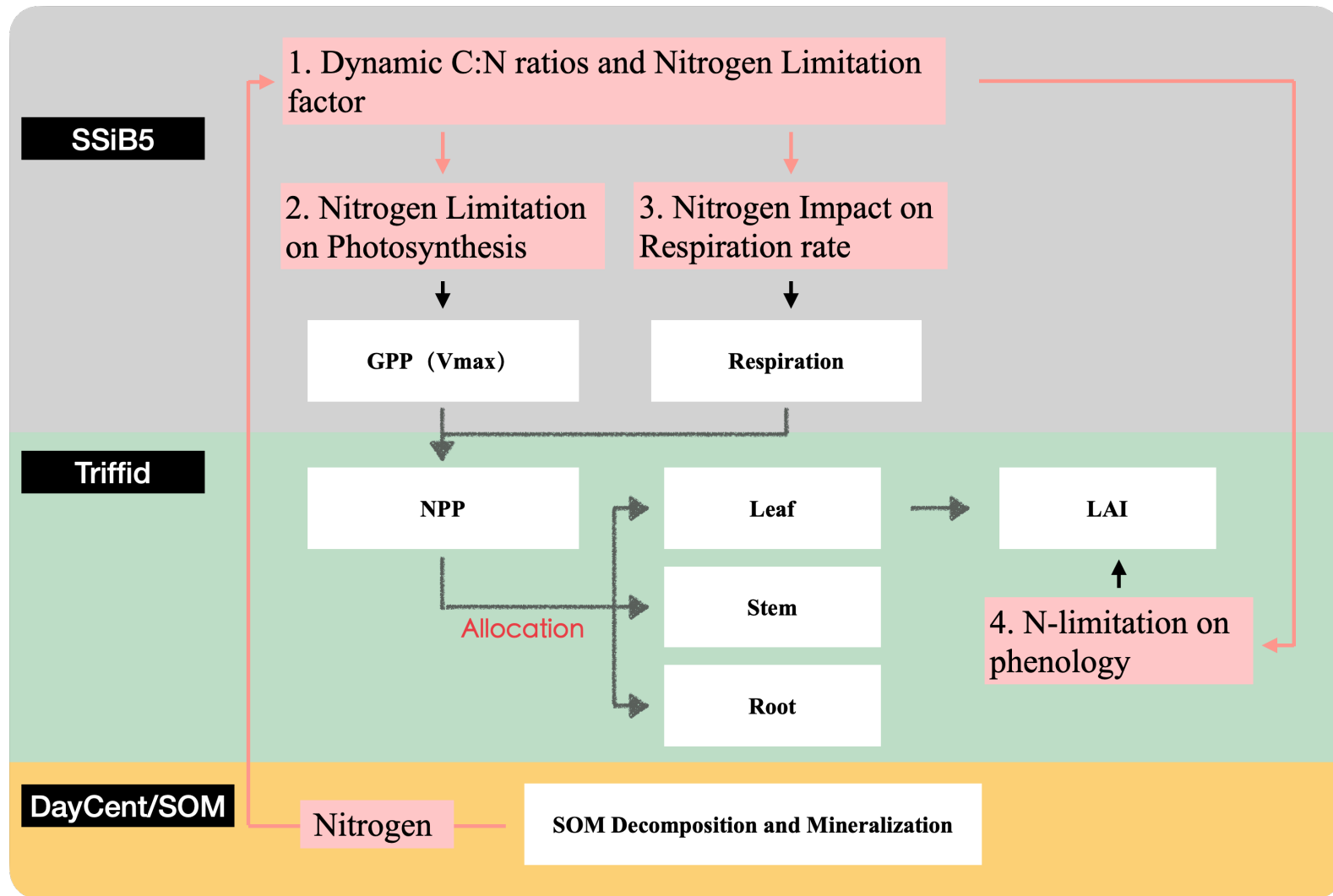


Figure 1. Schematic diagram of plant biogeochemistry and nitrogen impacts in SSiB5/TRIFFID/DayCent-SOM.

Notes: (1) Different background colors represent three different modules: SSiB, TRIFFID, and DayCent/SOM; (2) Boxes with white color indicate the main processes in C-N coupling in different modules; (3) Boxes with vermeil color indicates how the nitrogen influence plant biogeochemistry through our C-N framework.

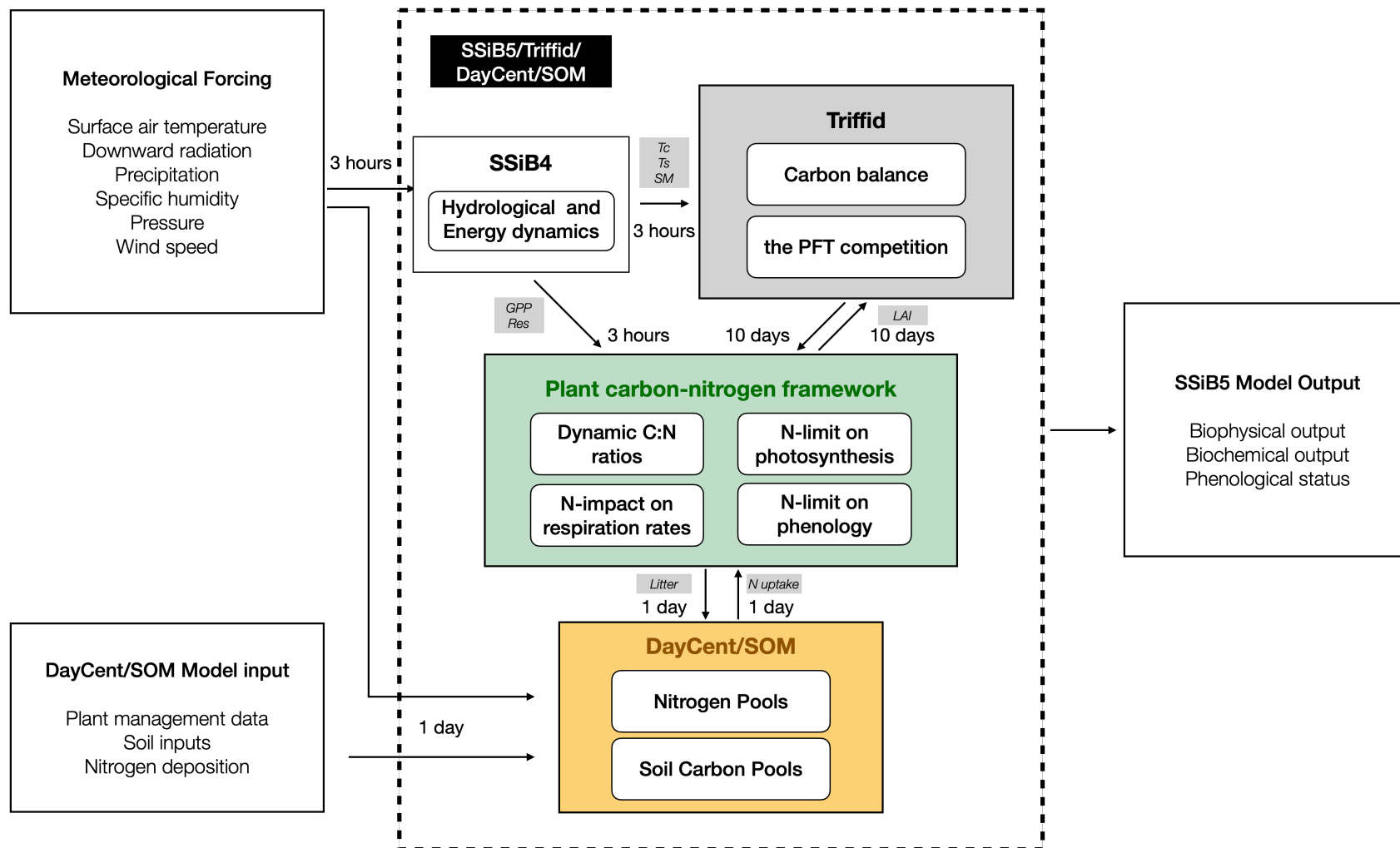


Figure 2. The flowchart of plant carbon-nitrogen interactions in SSiB5/TRIFFID/DayCent-SOM, main variables are listed between two modules

Notes: Tc: canopy temperature; Ts: land surface temperature; SM: soil moisture; GPP: gross primary productivity; Res: autotrophic respiration.

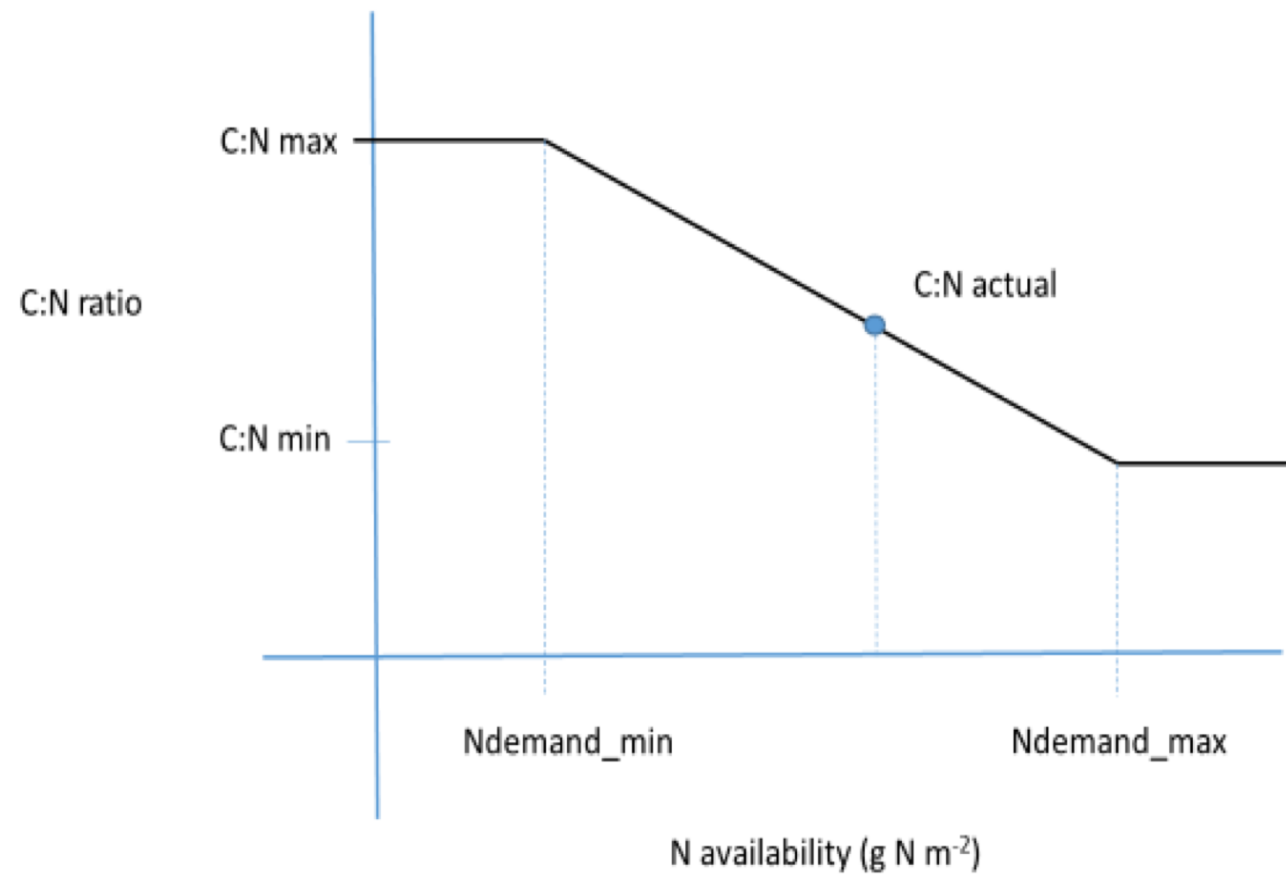


Figure 3. The relationship between the soil nitrogen availability and plant carbon-nitrogen ratios

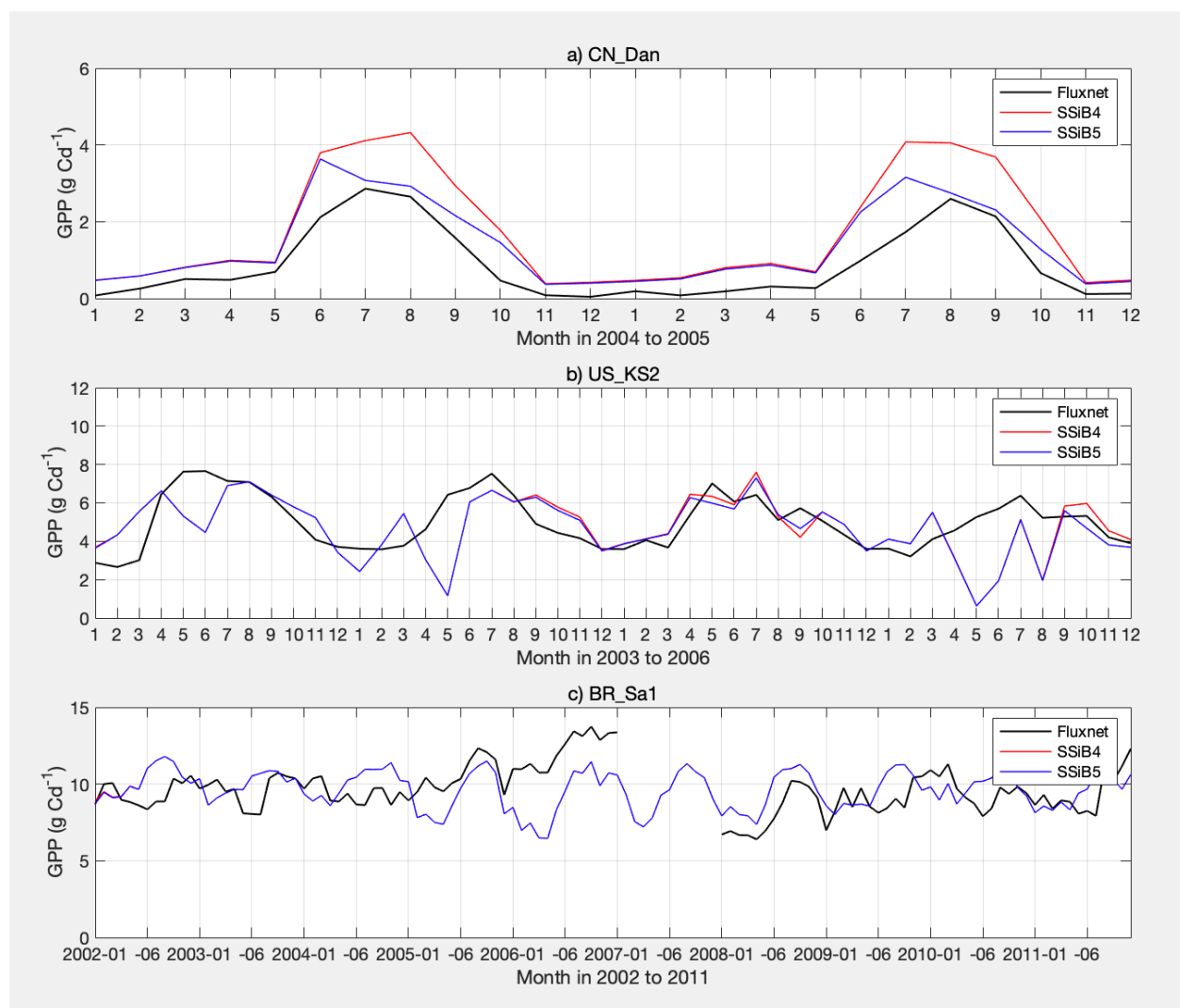


Figure 4. Simulated seasonal variations of GPP against observations at three FLUXNET sites representing different SSiB5 PFTs (C3 grass, broadleaf deciduous tree, and broadleaf evergreen tree).

Note: the information of three FLUXNET sites, CN_Dan, US-KS2 and BR-Sa1, are listed in Table 3.

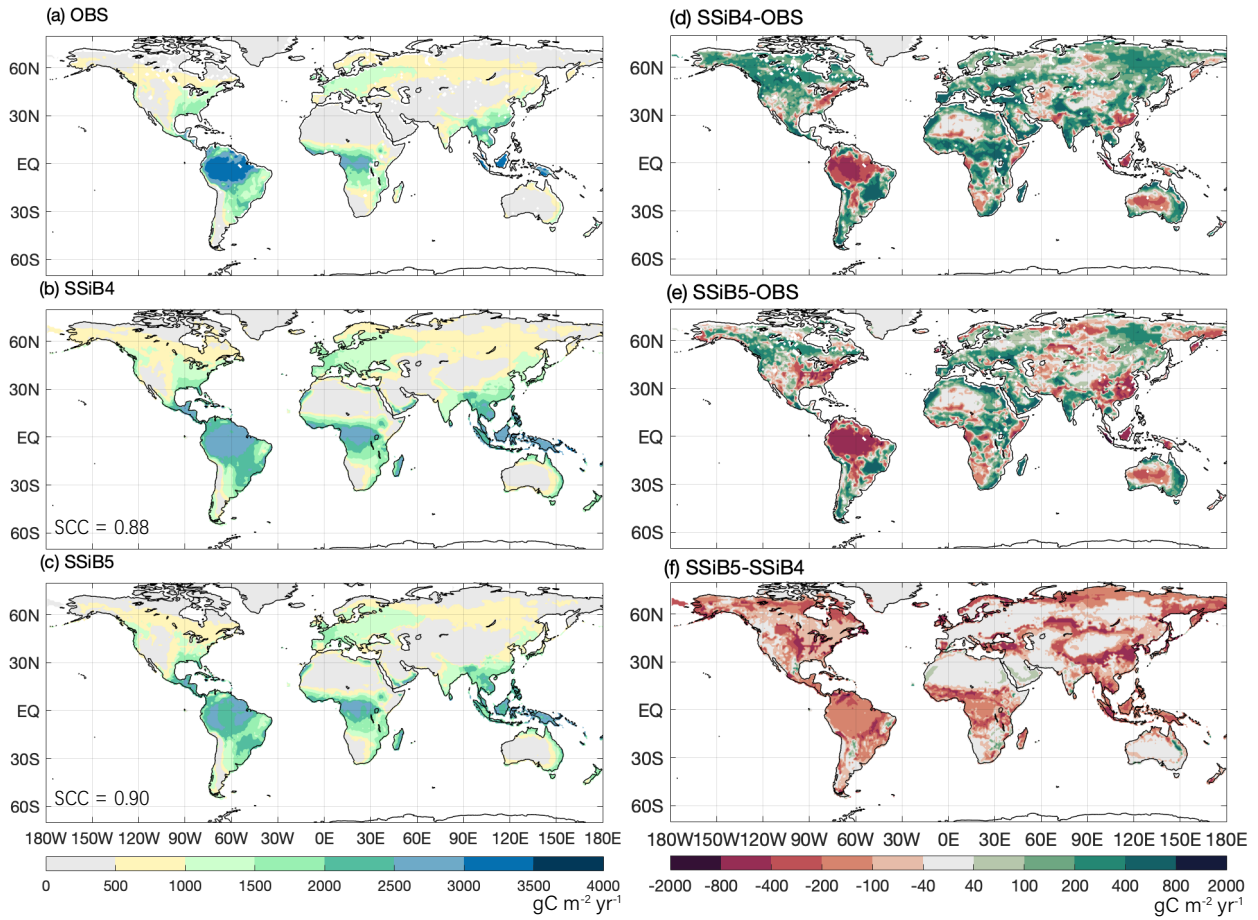


Figure 5. The 1982-2007 average gross primary production comparison for (a) FLUXNET-MTE GPP (OBS), (b) SSiB4/TRIFFID (SSiB4), and (c) SSiB5/TRIFFID/DayCent/SOM (SSiB5), and difference between (d) SSiB4-OBS, and (e) SSiB5-OBS, (f) SSiB5-SSiB4.

Note: SCC indicates the spatial correlation coefficient between model simulation and satellite-derived datasets (OBS).

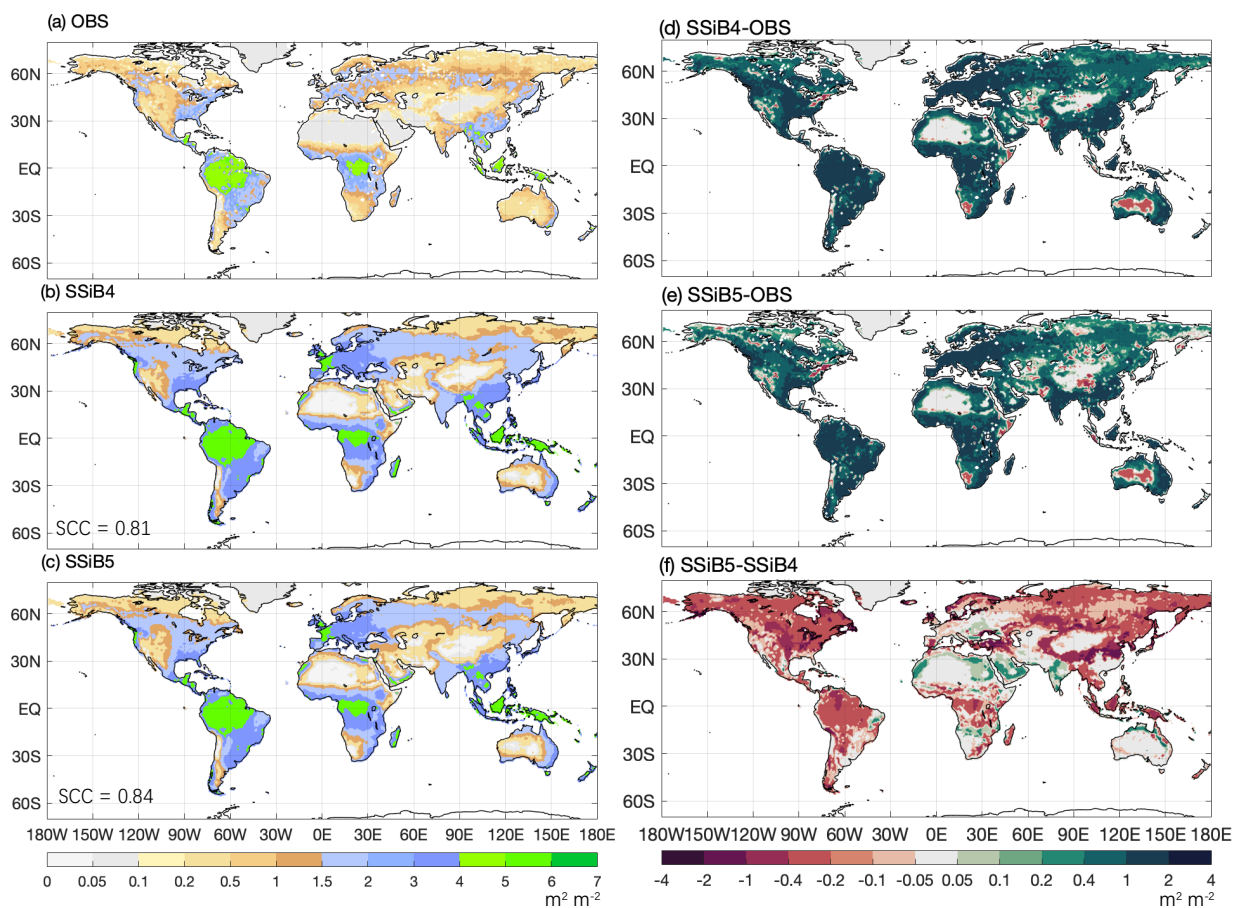


Figure 6. Same as Figure 5, but for LAI.

Note: SCC indicates the spatial correlation coefficient between model simulation and GIMMS LAI (OBS).

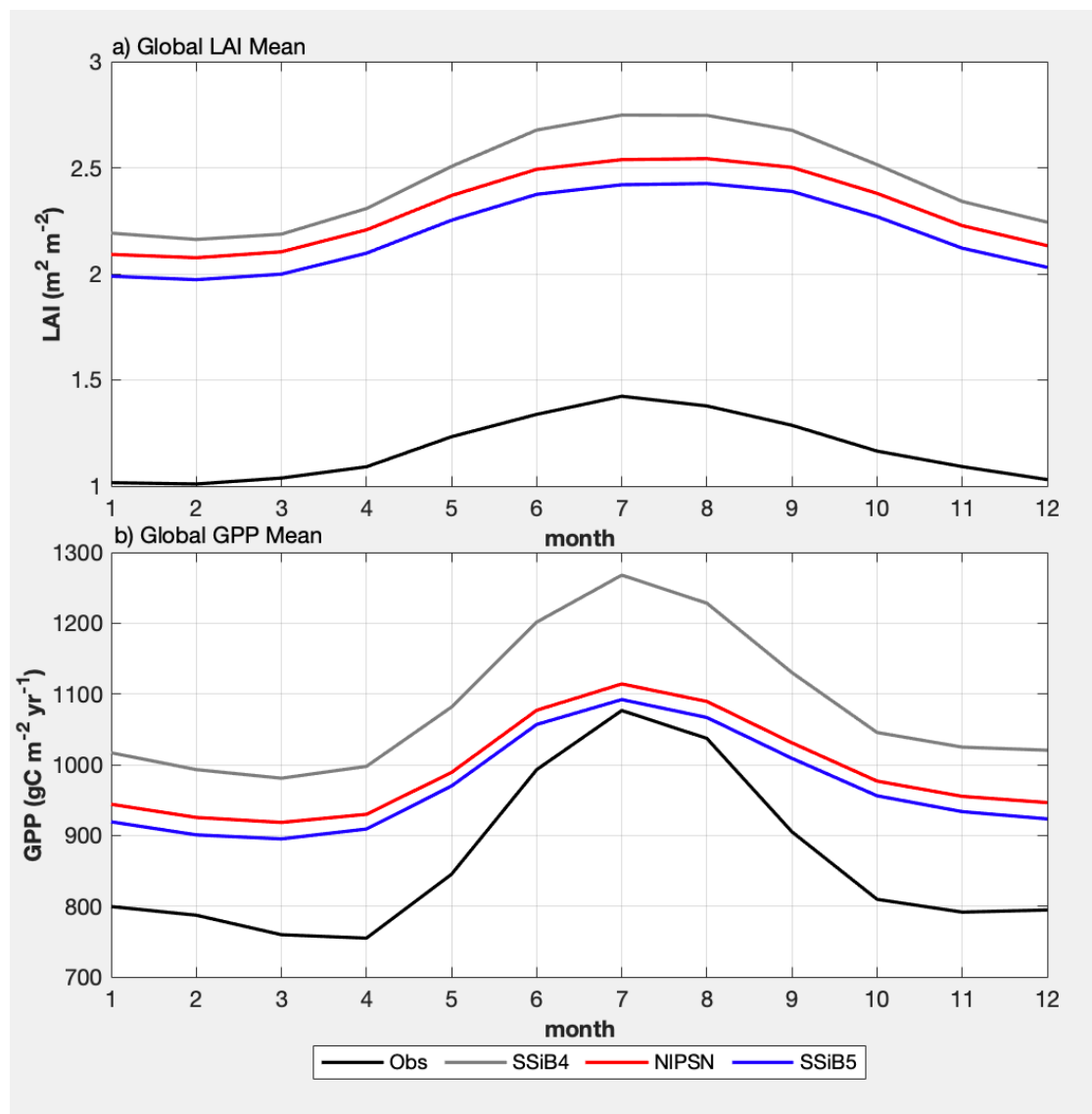


Figure 7. Intercomparisons of monthly LAI and GPP among OBS, SSiB4, NIPSN, and SSiB5 over the period 1982-2007.

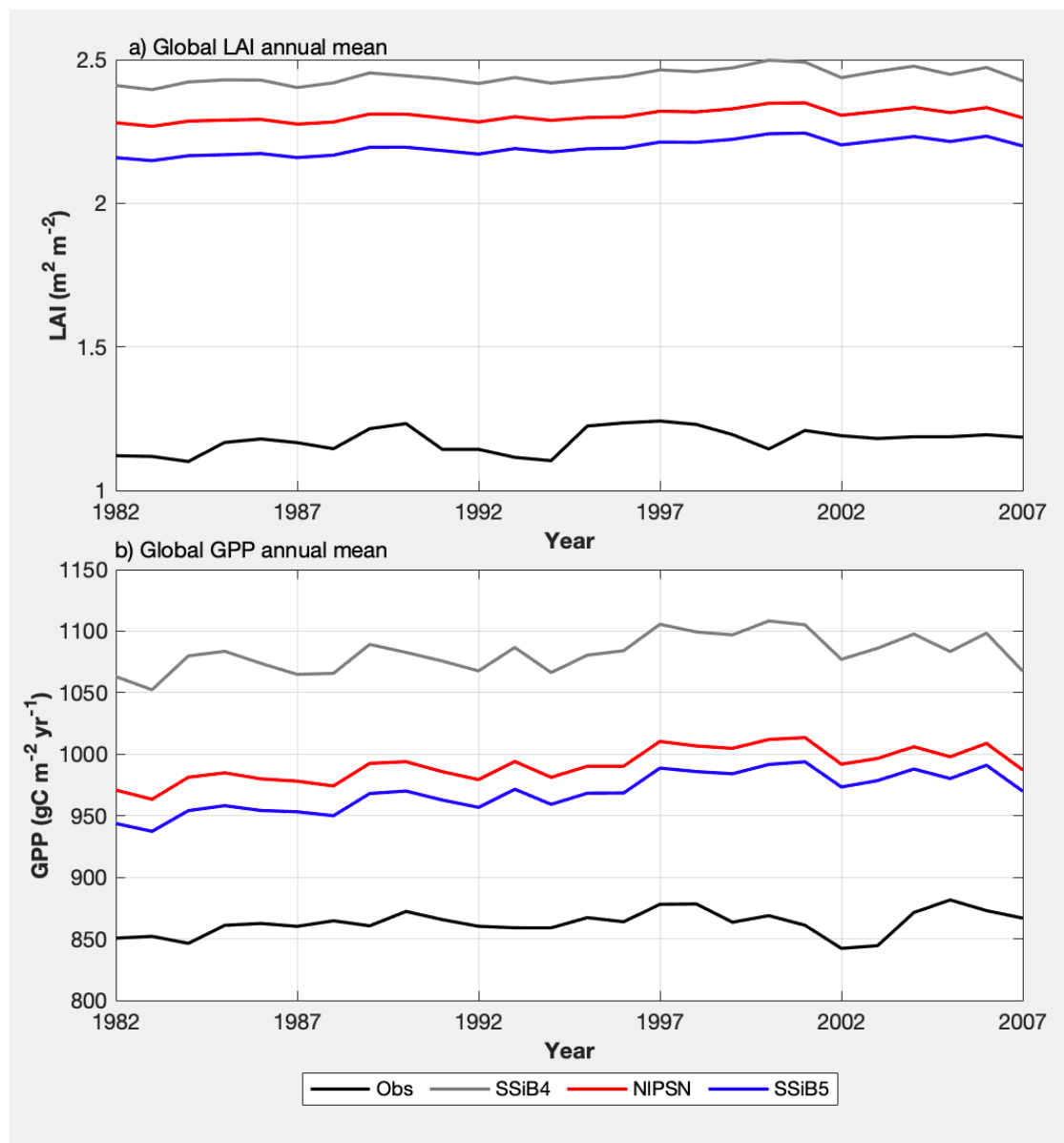


Figure 8. Same as figure 7, but for annual LAI and GPP.

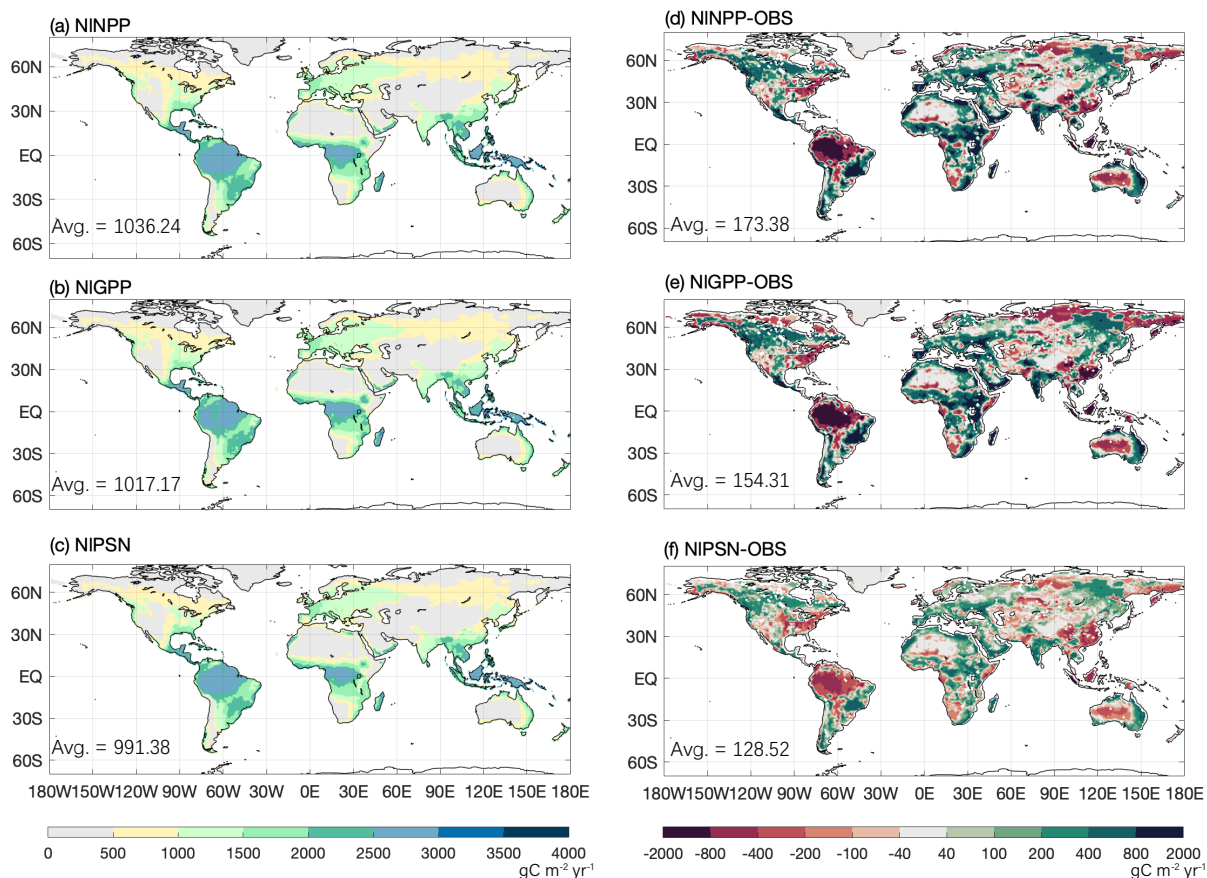


Figure 9. The 1982-2007 average gross primary production comparison for (a) NINPP, (b) NIGPP and (c) NIPSN, (d) NINPP- OBS, (e) NIGPP- OBS and (f) NIPSN- OBS.

Notes: (1) NIPSN is N limitation on photosynthesis (V_{max}) only; NINPP is N limitation on NPP only; and NIGPP is N limitation on GPP only. (2). OBS is FLUXNET-MTE GPP (OBS). (3). Avg. indicates the global average.

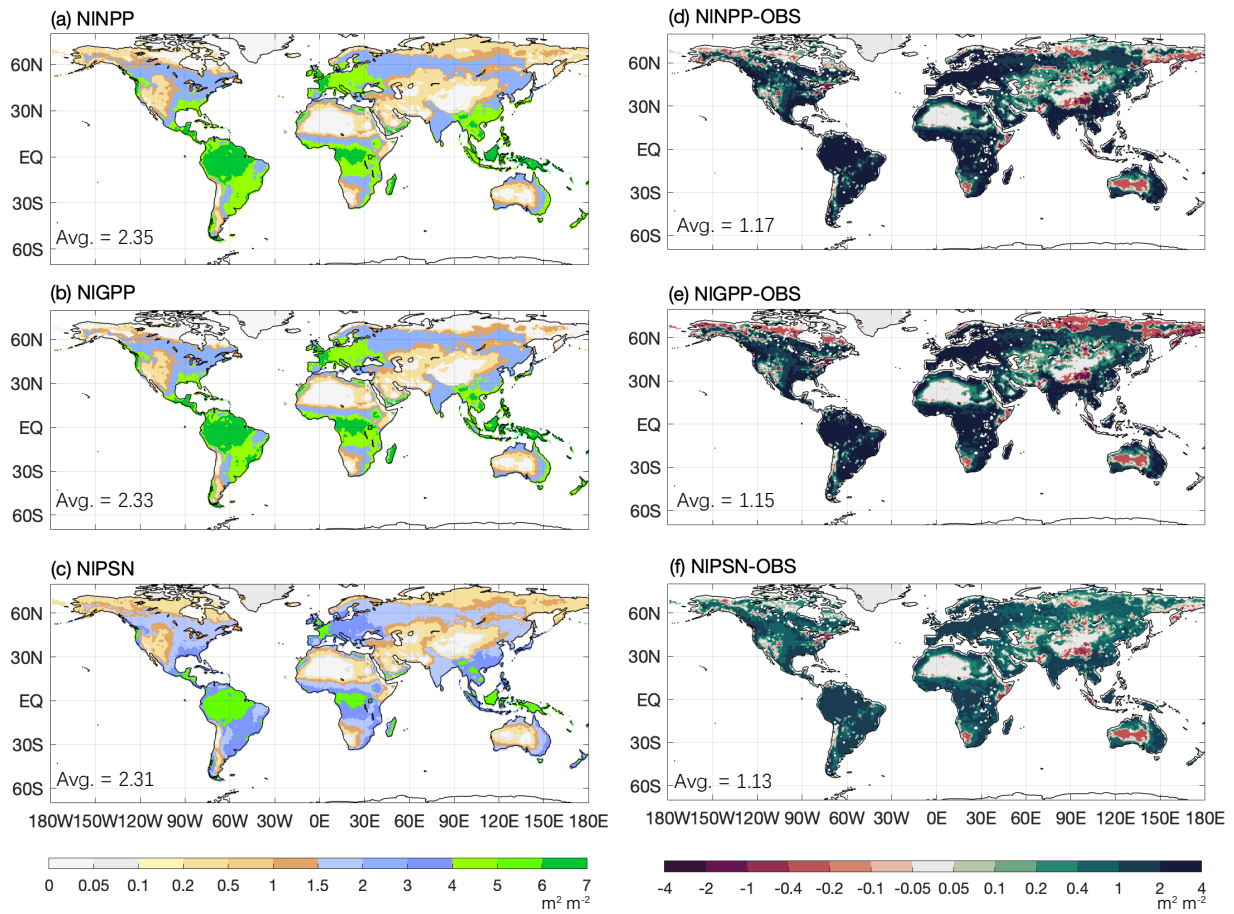


Figure 10. Same as Figure 9, but for LAI.

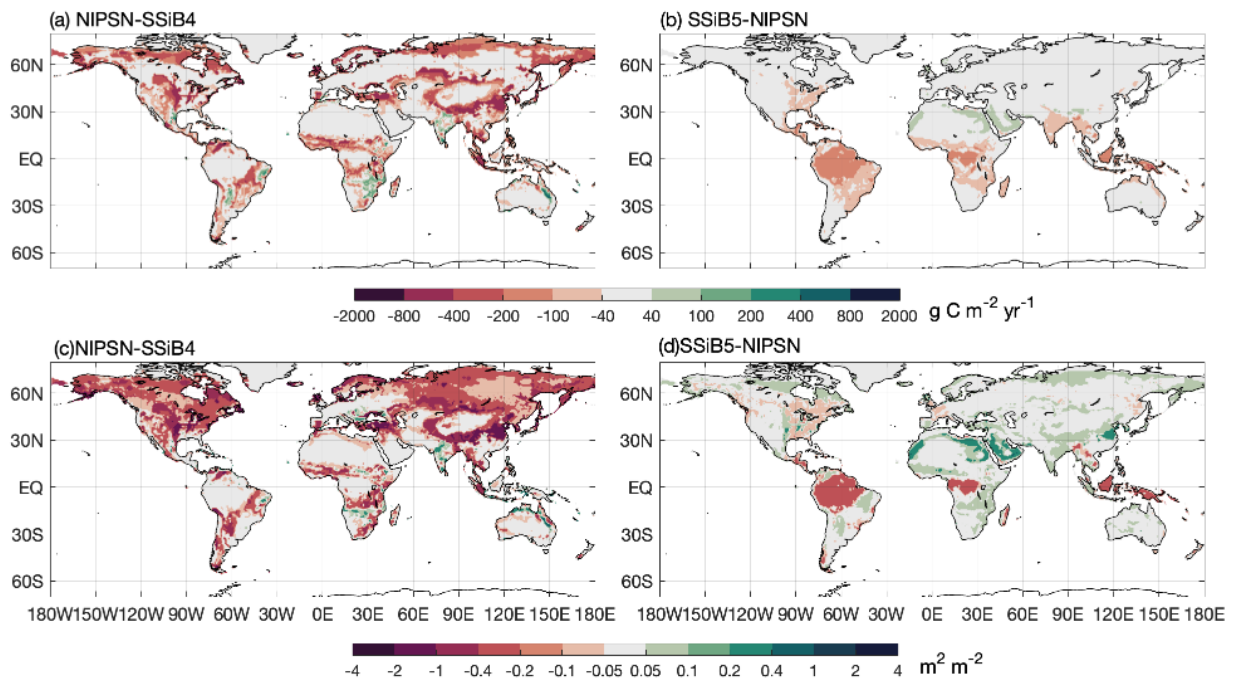


Figure 11. The 1982-2007 average gross primary production difference (a) NIPSN-SSiB4, (b) SSiB5-NIPSN, and leaf area index difference (c) NIPSN- SSiB4, (d) SSiB5- NIPSN

Note: NIPSN is N limitation on photosynthesis (V_{\max}) only.